UNIVERSITY OF ZIMBABWE

THEORY BOBO (R952241T)

MSC RENEWABLE ENERGY DISSERTATION

A MODEL FOR AN ECONOMIC HYBRID ENERGY SOLUTION FOR A MEDIUM SCALE GOLD MINE IN REMOTE ZIMBABWE

SUPERVISOR: ENG. T. HOVE

07 JULY 2017

ABSTRACT

The growth in energy demand is surpassing generation capacity especially in developing nations. Traditional energy sources such as fossil fuels are finite and are the largest contributors to global warming due to emission of greenhouse gases (GHG). Strong initiatives have been borne to address energy sources whilst embarking on sustainable energy policies to reduce GHG and hence retard global warming. In the developing world, energy has been identified as one of the key drivers for sustainable development. It is against this background therefore, that renewable energy sources especially solar, wind and lately battery storage are now being included in the energy mix to address energy shortages whilst curtailing global warming. To provide energy to remote areas hybrid energy systems, grid-connected or off-grid, are being developed, with an incorporation of renewables into the energy mix. However, in most cases, sizing of hybrid energy solutions are done intuitively resulting in many cases of oversizing of hybrid energy systems which increases the cost.

The objective of this study is to therefore develop a general model for sizing of an optimum economic and feasible hybrid energy solution for a grid-connected energy consumer. The model will offer a systematic approach to energy system sizing and will be applied to a remote gold mine in rural Zimbabwe. The model is developed in the constraint of a 100% supply reliability whilst reducing the levelised cost of energy. The model will also introduce renewable energy RE into the energy mix of the mine and thus reduce the direct GHG by the mine when diesel generators are used for back-up power in the absence of the grid. The hybrid energy solution is modelled in Microsoft Excel and customized to suit local conditions. The model is based on an energy demand matrix of the remote mine where the daily energy demand is 4.3MWh and peak load is 197kW.

List of Tables

List of Figures

NOMENCLATURE

β	Angle of tilt of a surface, degrees
$\beta^{/}$	temperature coefficient of efficiency for a PV panel, $^{o}C^{-1}$
δ	The suns angle of declination, degrees. Varies by day
φ	Latitude of site, degrees. North is positive and South is negative
η	Efficiency of a PV panel to convert solar radiation to electrical energy, %
η_r	Efficiency of a PV panel to convert solar radiation to electrical energy, %, at reference conditions – radiation of 1000 W/m^2, ambient temperature of 25^{o}C
θ	Angle of incidence on a plane, measured from the normal, degrees
θ_z	Angle of incidence of direct radiance on a horizontal plane, degrees
ω	the angular displacement of the sun east or west of the local meridian due to rotation of the earth on its axis at 15^{o} per hour – $\omega = 15(t-12)$
γ_s	Surface azimuth angle, the deviation of the projection on a horizontal plane of the normal to the surface from the local meridian, with zero due north, east positive and west negative; $-180° \leq \gamma \leq 180°$.
γ	Radiation intensity coefficient
G_{sat}	Satellite global irradiation, W/m^2
B_{gain}	Hourly energy gained by the battery, KWh
B_{cap}	Effective battery capacity, KWh
B_{state}	Battery energy level at the beginning of the hour, KWh
E_w	Hourly energy wasted in the system due to excess capacity and battery losses when battery is in the system
E_o	Hourly energy wasted in the system without battery storage, kWh
I_h	Hourly global irradiation on a horizontal plane, W/m^2

I_b	Hourly beam irradiation on a horizontal plane, W/m^2
I_d	Hourly diffuse irradiation on a horizontal plane, W/m^2
I_{array}	Hourly global irradiation on a PV plane, W/m^2
$I_{array,NOCT}$	Hourly global irradiation on a horizontal plane, W/m^2 at NOCT
K_{sat}	Satellite clearness index
K_{gr}	Ground clearness index
L_s	Hourly solar energy delivered to the load, kWh
L_o	Hourly energy demanded by the load, kWh
L_{day}	Daily energy demanded by the load, kWh
L_s	Hourly solar energy delivered to the load, kWh
N	Day number of the year
R_b	The ratio of beam radiation on a tilted surface to that on a horizontal surface
T_r	Reference cell temperature for efficiency, ^{o}C
T_c	Cell temperature, ^{o}C
$T_{C,NOCT}$	Cell temperature at nominal cell temperature (NOCT) conditions, ^{o}C
T_a	Ambient temperature, ^{o}C
$T_{a,NOCT}$	Ambient temperature at nominal cell temperature (NOCT) conditions, ^{o}C

ACRONYMS

AC	Alternating current
DC	Direct current
DG	Diesel Generator
GDP	Gross Domestic Product

HES	Hybrid Energy System
HOMER	Hybrid Optimisation Model for Energy Renewable
IAB	Incremental Annual Benefits
IAOC	Incremental Annual Operating Costs
ICC	Incremental Capital Costs
IEA	International Energy Agency
IPCC	Inter-Governmental Panel on Climate Change
IPP	Independent Power Producers
MPPT	Maximum Power Point Tracking
NPV	The Net Present Value of life cycle savings
NREL	National Renewable Energy Laboratory
OPEC	Organisation of the Petroleum Exporting Countries
PV	Photovoltaic
REs	Renewable Energy
RE Fraction	Annual average renewable energy contribution to the load
SADC	Southern African Development Community
SAPP	Southern Africa Power Pool
SFC	Diesel generator specific fuel consumption
WB	World Bank
ZETDC	Zimbabwe Electricity Transmission and Distribution Company
ZPC	Zimbabwe Power Company

ACKNOWLEDGEMENTS

I extend my sincere gratitude to my supervisor and lecturer Eng. Tawanda Hove whose guidance and critiquing challenged and shaped me. I would also like to thank all of my lecturers in the MSc Renewable Energy Program.

To Mr. Thomas Gono, senior partner at Gold Reef Mine, owners of Ruia Mine used as a case study in this research, and his Ruia Mine staff, I extend my heartfelt gratitude.

To my fellow classmates, the sharing of ideas, the discussions – yes we came this far together.

I acknowledge with much gratitude the unconditional support my family gave me in the two years – Felistus my wife, our children Anesu, Nyasha and Tendekayi – for the sacrifice. I could not have come this far without your love.

Above all, I thank God for everyone. May God continue blessing you all in your endeavors!

Chapter 1 Introduction

1.1 Introduction – Electrical Energy Status in Zimbabwe

Electrical energy consumption in Zimbabwe has experienced significant increase attributed to population growth – growth in domestic consumers, the small to medium enterprises (including small scale mining and agriculture) and the informal sector industry (ZimSTATS – Digest of Statistics Quarter 4 2016) . Electrical energy consumption was reported higher than generation capacity leading to net importation of electricity from the SADC countries – South Africa, Mozambique and Zambia - of up to 350MW according to statistics from the ZPC (www.zpc.co.zw – generation statistics as of 09 May 2017).

The electrical energy shortfall has been exacerbated by the drop in generation capacity due to derating of some generators, from a total of 2045MW at commissioning to 1910MW, short supply of thermal coal for the coal based power stations (Bulawayo, Harare, Hwange and Munyati) as well as drought induced effects on Kariba hydropower generation (www.zpc.co.zw). Consequently, power generation stood at 1131 MW as of 09 May 2017. Zimbabwe's electricity tariff averaged 9.83USc as of 09 May 2017/ kWh (www.zesa.co.zw) making it the second highest electricity tariff in the SADC region.

The current electrical power import of 350MW is insufficient to meet electrical demand estimated at 2600MW by 2004 (Reserve Bank Quarterly Review, 2002). Thus, the country's power utility embarks on scheduled load shedding on a rotational basis country wide (www.zesa.co.zw) to manage power demand. Load shedding due to the failure of the utility's to provide adequate electrical power has negative impacts on industrial operations. In the period 2011 to 2015, the country's declining economy marked by reduced manufacturing activity and depressed minerals commodity prices have reduced foreign currency inflows into Zimbabwe (RBZ Monetary Policy Statement, Sept 2016).

Shortage of foreign currency is a potential major threat to future electrical power imports. It can also be argued that if industrial capacity utilization was at pre-2000 levels, the electrical energy supply will even be more severe resulting in more frequent and longer duration of load shedding in the country – the electrical supply utility would not supply adequate energy to meet the energy needs.

On the other hand, some industrial consumers, including those in remote areas, operating on 24 hours a day or those seeking to secure their electrical power needs have included diesel generator (DG) sets into the electrical energy mix to increase supply reliability. Whilst DGs increase supply reliability, the resultant electrical energy for the operation is expensive and contributes to the emission of greenhouse gases which works against the resolutions of SADC and of COP21 to adopt plans that will highlight actions individual countries will take to reduce GHG emissions and hence keep global warming below 2°C (www.CO21.paris.org). Supply of diesel fuel for the DGs is a logistical challenge for remote industrial consumers in a landlocked country such as Zimbabwe and is exposed to the threats of potential foreign currency shortage as well as the prevailing high prices to purchase the fuel in Zimbabwe.

In light of the fore-going, the cost of loss of production at a remote industrial operation due to lack of electrical power is higher than the electrical cost. DGs have thus become a common feature in most energy mixes to keep operations running 24/7 and maintain productivity.

It is against this background therefore, that other energy sources are being explored and employed to increase energy reliability whilst lowering the cost of energy. Renewable Energy sources have been included in the energy mixes into a micro-grid network - both on-grid and off-grid applications - to ensure reliability of energy supply as well as in mitigating the effects of global warming. “*A Micro-grid is described as a local energy*

network which offers integration of distributed energy resources (DER) with local elastic loads, which can operate in parallel with the grid or in an intentional island mode to provide a customized level of high reliability and resilience to grid disturbances. This advanced, integrated distribution system addresses the need for application in locations with electric supply and/or delivery constraints, in remote sites, and for protection of critical loads and economically sensitive development". (Myles, et al. 2011)

A remote grid connected industrial operation, a remote gold mine in Zimbabwe has been identified as a case study to model a hybrid energy solution which ensures reliability of energy supply, include a significant renewable energy (RE) penetration in the energy mix and thus promote a low-carbon electrical energy consumption for the mining operation, reduce greenhouse gases emission, lower energy cost and ultimately promote energy security.

Solar power is the RE source to be added to the grid and together with DG would be in a hybrid mix modelled with battery energy storage. The costs of solar power generation are falling globally. Falling solar project costs have recently been reported making it an attractive renewable energy option - analysts have reported modules quotes of between \$0.40 and \$0.50/W_p and some in the industry have seen quotes below \$0.40/W_p for 2017 delivery (Runyon, 2017). The reduction in installation prices per kWh are attributed to the improvement in panel efficiencies and government supports. In the early months of 2017, record low tenders for projects in India, Dubai and Chile were reported. Costs of energy storage are also falling (Runyon, 2017).

A hybrid energy solution with a high renewable energy penetration will therefore support SADC and hence Zimbabwe's drive to increase power generation from renewables; indeed SADC's objective is to have 32% renewable energy source by 2020 and 35% by 2030 (www.sadc.com).

1.2 Problem Statement

In a situation where there are power outages from the utility (load shedding), the reliability of power supply is low resulting in loss of revenue due to downtime for industrial operations even though the cost of grid electricity is low at 8c/kWh.

As per the schedule of 2014 for Northern Region, Bindura District, the grid does not supply electricity for 64 hours per week and thus reliability of supply is only 62%. (www.zetdc.co.zw – load shedding Northern Region, Bindura District). Extrapolated to a year, that represents a significant loss of revenue for the selected case study.

In such situations, operators sacrifice by using high cost diesel generation to back up power supply and sustain production. Whilst the operations will keep running, electrical energy cost rise and the operation increases its carbon-footprint and directly emit greenhouse gases owing to the consumption of fossil fuel in electricity generation. Further, given the volatility of the diesel prices on the world market and the logistical challenges in supplying diesel fuel to the remote mine for the back-up electricity, it is important to note therefore that DGs are not an economical and sustainable energy solution to secure the energy requirements of the mining operation.

1.3 Justification

The author justifies the development of a hybrid energy system (HES) model in order to achieve the following;

- Reduced the mine's direct carbon footprint and hence highlight the mine's responsiveness towards sustainable development
- Reduced LCOE compared to the natural choice of using diesel generators
- Increased energy security through incorporation of multiple energy sources

- Increased global use of renewable energy sources in industrial operations and reduced use of finite conventional energy sources
- Development of an HES sizing model which can be replicated to other similar operations

1.4 Purpose of Study

1.4.1 Aim

The aim of this study is to design a HES model to increase power supply reliability at the lowest possible cost of energy

1.4.2 Objectives

The main objectives of the study are to:

- To design a computer based tool that can simulate the reliability and energy cost of an HES
- Secure the electrical energy supply to the mine - 100% reliability
- To use the LCOE as an objective function to minimise while meeting the constraint of a 100% reliability
- To produce generalised design curves and LCOE functions for grid-connected HES with the similar load profiles
- To prescribe an HES model for a case study - Ruia Mine

Chapter 2 Literature Survey

2.1 Global Energy Supply

The global energy demand continues to growth at a projected 30% until 2040 through growth in population, industrialization and urbanization. Global energy consumption is significantly driven by China, India, Africa, Latin America and Middle East. In Sub-Saharan Africa, it is estimated that slightly above 500 million people in rural areas will remain without electricity by 2040 compared to the present 1.2 billion people (IEA - World Energy Outlook 2016).

The growth in energy demand foresees also the rise in consumption of fossil fuels which are finite with a possibility of switching fuels to meet energy needs. It is estimated that natural gas consumption will rise by 50% and oil consumption rising to a maximum of 103 million barrels / day by 2040. In the forecast, coal and oil consumption will be affected by the environmental concerns which aim at curbing global warming enforced by the signing of the Paris Agreement on Climate Change in November 2016 by about 190 countries (IEA - World Energy Outlook 2016).

The Paris Agreement on climate change's objective is to control global warming and cap temperature rise to below $2^{o}C$. Prior to the agreement it has been noted that the energy sector contributes up to two-thirds of the total greenhouse gas emissions and that transformation is required in the energy sector. Therefore, it has an impact on the global trends, future energy investments and policies.

A stall in growth of energy related CO_2 was reported in 2015 driven by an emerging focus on a low carbon economy and improved energy efficiency. Uptake of renewable energy sources into the global energy-mix has seen significant growth, accounting for up to 20% until 2015. In the same period, investments in Oil and Gas fell in value from $500 billion in 2014 to $325 billion in 2015 (IEA - World Energy Outlook 2016).

.

Thus the impact of the energy deficit driven by demand, dwindling of traditional fossil fuels and the environmental pressures will drive uptake of renewable energy sources. To this end, China and India have experienced the most significant growth in photovoltaics (IEA - World Energy Outlook 2016).

2.2 Africa Energy Supply

2.2.1 General Overview

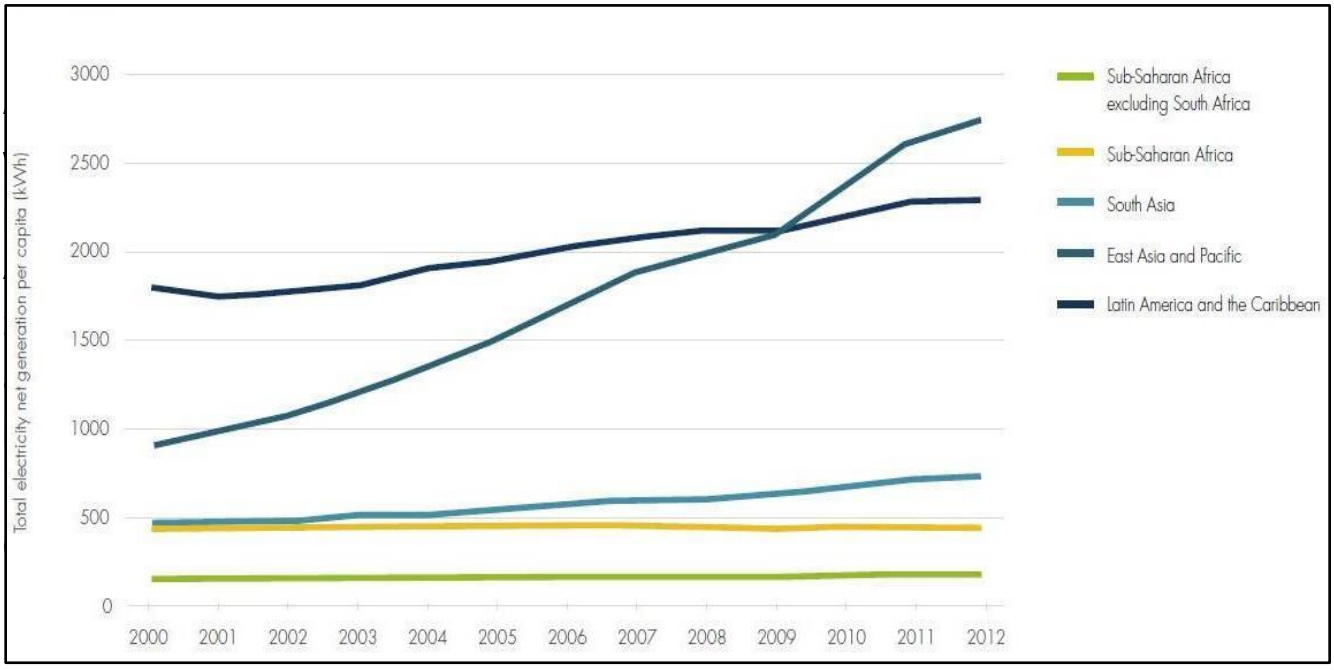

Fig 2.1: Total Electricity Net Generation International Energy Statistics - U.S. Energy Information Administration (2012).

The poor population in remote areas remains the most vulnerable as the highly centralised energy systems designed to benefit the rich and bypass the poor. Power utilities have been centres of political patronage and corruption, Africa Progress Panel (2015). Further, the installed generation facilities have seen capacities trending downwards due to aging equipment requiring capital injection and frequent maintenance and on the other hand droughts due to climate change affecting hydropower capacity.

The continent is also challenged by the reality of climate change. Electricity access has to be expanded sustainably to meet energy needs, sustain economy growth, create jobs and alleviate poverty while respecting environmental commitments made to combat climate change. Energy policy is central in Africa meeting its development goals, Africa

Progress Panel (2015). The energy question in Africa therefore links energy, poverty and climate change, Africa Progress Panel (2015). Thus it is widely noted that the Africa's leadership has to implement energy policies that address energy equity deficiencies with a strong bias towards renewables in driving the energy-mix due to their abundancy.

2.3 HES – Global Deployment Status, the Trends

Hybrid energy technology has improved through the advances in control systems to address intermittences, system balancing when connected to the grid as well as quality problems. Battery energy storage system has also enjoyed a reduction in prices – including lead-acid and lithium-ion batteries. Bloomberg New Energy Finance expects battery technology to fall to $120 per kWh by 2030 compared with more than $300 now and $1,000 in 2010. The economics for a hybrid energy solution is therefore becoming justifiable.

Some countries such as Peru, Kenya, Nepal, Indonesia and Sri Lanka have experienced higher rates of electrification and thus while increasing electrification rates might technically reduce the market's attractiveness for off-grid operators, the statistics often ignore that many newly connected households receive only an irregular power supply (Bloomberg New Energy Finance, Q1 2017 OFF-GRID AND MINI-GRID MARKET OUTLOOK, 18 JANUARY 2017). This therefore, supports the need to harness REs into hybrid energy solutions even for grid-connected remote industrial operations.

Further, incorporating REs into the energy mix reduces the electrical generation by the DG and hence diesel consumption whose supply is threatened by price fluctuations and

are finite sources. For example, energy storage players Electro Power Systems has secured an equipment contract to deliver 313kWh of storage technology for a mini-grid run by a local utility in Somalia, helping to reduce costs by replacing diesel generators with a 1.7MW wind installation (Bloomberg New Energy Finance, Q1 2017 OFF-GRID AND MINI-GRID MARKET OUTLOOK, 18 JANUARY 2017).

Falling solar project costs have recently been reported making it an attractive renewable energy option - analysts have reported modules quotes of between \$0.40 and \$0.50/W_p and some in the industry have seen quotes below \$0.40/W_p for 2017 delivery. The reduction in installation prices per kWh are attributed to the improvement in panel efficiencies as well as governmental support (Renewable Energy Magazine 2017).

The following two tables summarise the deployment of HE - Solar and Wind (where applicable) and Energy storage globally in the past year 2016:

- Selected community mini-grids announced in 2016
- Selected commercial and industrial applications announced in 2016

Country	Project	Parties involved	Capacity (PV in kW / storage in kWh)	Date Announced
Nepal	Three mini-grids to serve a mobile tower as anchor load and nearby villages	N-Cell, Gham Power, Asian Development Bank	30	26 July
Madagascar	Deliver power to 100 remote villages / 0.4m people	Fluidic Energy, Caterpillar, Government of Madagascar	7,500 / 45,000	24 August
Somalia	Expansion of a hybrid off-grid power plant in Garow, capital of Puntland state, supplying	Electro Power Systems, National Energy	1,700 (wind) / 313	29 July

	more than 100,000 people with wind power and diesel.	Corporation of Somalia		
Tanzania	EUR 16m Ukara Island system serving 250 customers, to be expanded to other villages on the island.	Jumeme Rural Power	60 / 240	12 April
Kenya	Supported by a EUR 33m credit from the French government, Kenya plans to build 23 solar and one 0.6MW wind mini-grid across seven counties in northern Kenya	Kenya Power, French government	9,600 and 600 (wind) / n.a.	10 August
Mali	50 solar and storage containers to be deployed across 25 villages in rural Mali	Africa Green Tec, Tesvolt	~2,000 / 3,000	22 November
Democratic Republic of Congo	A foundation affiliated with Tesla (formerly SolarCity) has built a renewable mini-grid powering facilities at Virunga National Park. The project used Tesla's energy storage products.	GivePower Foundation	50 / n.a.	25 August
American Samoa	Tesla (formerly SolarCity) announced it had retrofitted a diesel-powered mini-grid on the island of Ta'u with solar and lithium-ion batteries.	Tesla	1400 / 6,000	22 November

Table 2.1 Selected community mini-grids announced in 2016, Bloomberg New Energy Finance, Q1 2017 OFF-GRID AND MINI-GRID MARKET OUTLOOK, 18 JANUARY 2017).

Country	**Project**	**Parties involved**	**Capacity (PV in kW / storage in kWh)**	**Date Announced**
South Africa	ABB installed a grid-connected solar diesel mini-grid on its own premises in Johannesburg. The project integrates renewables in its power supply and shields the site from grid outages.	ABB	750 / 380	8 June 2016
Kenya	Solar-plus-storage mini-grid at	Aquion Energy, Solar Africa	37 / 106	12 July 2016

	Loisaba Conservancy replacing 95% of diesel use.			
Rwanda	134 lithium-ion storage systems to complement a 3.3MW solar array at a farm in Eastern Rwanda. The power is primarily used to run water pumps during grid outages.	Tesvolt, Ideema Sun	3,300 / 2,680	14 June 2016

Table 2.2 Selected commercial and industrial applications announced in 2016, Bloomberg New Energy Finance, Q1 2017 OFF-GRID AND MINI-GRID MARKET OUTLOOK, 18 JANUARY 2017).

"*A new approach is needed for the grid of the future; a grid that can support remote mining and industrial sites and communities, and that can manage the peaks and troughs of energy demand, and a grid that can support the need for a greener planet*." (http://homerenergy.com/pdf/ABB-Microgrids-Brochure.pdf - ABB Microgrid Solutions: Advancing Sustainable and Reliable Energy Solutions).

Examples of where this new approach to electrical energy provision has been applied include Marble Bar and Nullagine where combined PV-DG power stations were commissioned in 2010 in the towns of Marble Bar and Nullagine, in Western Australia and represented the world's first high penetration of renewables into the energy power mix. The projects were comprised of more than 2,000 solar modules equipped with solar tracking. When the PV generation is low, DGs are ramped up to provide back-up power ensuring the network has a 100% power reliability. The solar energy systems generate over 1 gigawatt hour (GWh) of renewable energy per year, supplying 60 percent of the average daytime energy for both towns, saving 405,000 litres of fuel and 1,100 metric tonnes of greenhouse gas emissions each year (ABB Microgrid Solutions: Advancing Sustainable and Reliable Energy Solutions).

The third-largest producer of nickel concentrate in the world, BHP Billiton owned Leinster nickel mine in Western Australia extracts ore from 1,000 meters underground with a large, electrically-driven winder which, at 8.5 megawatts (MW) of demand shift over 120 seconds, is a large cyclic load, given the unit's average power consumption is just 2 MW. "*To upgrade the winder's power supply, BHP temporarily installed a 1 MW PowerStore system, which reduced the total demand shift to 6.5 MW while adding 1 MW of spinning reserve to the system featuring a flywheel-based energy storage system which provides peak shaving and overcomes transient and cyclic loads on grid-connected or isolated systems. Whilst ensuring power supply reliabilty, the mine was able to increase winder production. PowerStore is fully automated and delivers power to the winder when it's needed most, and provides high-resolution data of winder performance and local electrical grid disturbances"* (ABB Microgrid Solutions: Advancing Sustainable and Reliable Energy Solutions).

2.4 Advances in Hybrid Energy Systems

The advances made in the development of solar as a renewable energy for electricity were reviewed by many researchers. Raja et al (1996) reviewed solar applications in Pakistan. Their work also gave recommendations on energy solution to the energy crisis facing Pakistan and the solutions included incorporating RE sources into the energy mix.

Ramachandra et al (1997) on their work assessing wind as an energy source in Uttara District in India concluded that wind energy could be utilized as a renewable energy source in rural remote areas and hence Kellog et al (1998) developed energy strategies for developing hybrid renewable energy system based on solar and wind.

Wind and Solar are considered viable renewable energy sources for powering remote off-grid areas to meet the growing energy demands and significantly reduce the greenhouse gases emissions as Dihrab and Sopian (2010), Dursun et al (2013), Nandi and Ghosh (2010) and Shaahid and I. El-Amin (2009) pointed. They concluded that REs meet energy needs sustainably, reduce GHS emissions, reduce maintenance costs and reduce overall cost of energy. However due to their intermittent nature related to climatic conditions, different REs are to be integrated in the HES which is referred to as a mix of optimized energy sources working independently to meet the energy requirements of the load according to Wang (2006).

Nandi and Ghosh (2010) found out in their work that different but optimized HES reduce the overall energy cost, improve the reliability of electrical energy supply thereby reduce the energy storage requirements compared to a system with a single RE source. Further work by Kusakana and Vermaak (2013) in the telecommunications sector found out that for remote stand-alone energy systems, hybrid PV-Wind-DG offer an economically feasible energy solution over the use of stand-alone conventional diesel generation option.

When renewables are incorporated into an HES, DG run-time is reduced thereby reducing operation and maintenance costs and GHG emissions. Inclusion of the BESS reduces the frequency of start and stops of diesel generators thereby reducing the specific fuel consumption (Jacobus et al. 2011).

Olatomiwa et al (2014) carried out an optimal Sizing of Hybrid Energy System for a Remote Telecom Tower in Nigeria. Their study concluded that PV-BESS-DG was an economical viable solution for the remote BTS. Jeffy Marin Jose and Cherian (2015) reviewed the design and cost analysis of hybrid power solution for grid connected remote telecom towers in India. In their study they focused on both off-grid and on-grid telecom sites as the grid were not a reliable power source for the remote sites.

Further studies were also made on grid connected HES, investigating generation and storage of energy in grid connected systems. Denholma and Margolis (2007) proposed energy storage in PV integrated energy systems to address the intermittence in PV energy supply and supply power during night hours when there is no PV generated power.

Babu and Ashok (2009) presented a study on the optimal utilisation of RE for industrial load management in peak load reduction and hence electricity charge using non-linear programming technique. The case study carried out in twenty two large scale industries showed a reduction in peak demand by 34% whilst electricity cost reduced by about 14 % when RE produced by independent power producers (IPP) was optimally utilized.

Riffoneau et al (2011) presented an optimal power management mechanism for grid connected PV systems. They proposed that power flow management can be a solution to manage intermittence of power supply in lieu of investment and operational costs associated with energy storage systems. The proposal focusses on the optimization of the HRES components in relation to local production in PVs and local consumption.

Daud et al (2012) presented an evaluation of performance for a grid-connected PV system with battery energy storage system. In their presentation, the BESS is equipped with a control mechanism for the state of charge and hence managing the charge/discharge of the BESS and the control mechanism will ensure a safe and efficient performance and safe operation of the BESS.

Norttott et al (2013) presented a linear programming (LP) routine based model for the optimal BESS dispatch strategy schedules for peak load management and the respective energy charge in a grid-connected, combined photovoltaic-battery storage system (PV -

BESS system). Their study included a cost benefit analysis of dispatch strategy based on mainly two constraints; battery storage capacity and peak load reduction with a target to obtain energy cost for the time-of-use and the net present value (NPV) of the BESS.

The financial benefits of the optimized energy dispatch schedule were compared with basic off peak charging/on-peak discharging and real-time load response dispatch strategies that did not use any forecast information, Norttott et al (2013). The NPV of the BESS increased significantly when the battery was operated on the optimized schedule compared to the off-peak/on-peak and real time dispatch schedules, Norttott et al (2013). With optimized dispatch strategy, battery service life increased whilst demand energy costs reduced.

In the Zimbabwean context, Hove and Tazvinga (2012) presented a technical and economic model for optimising off-grid HES component systems. The model applied sizing curves based on dimensionless generator component size variable, dimensionless Area component, supply reliability and diesel dispatch strategy. Their paper present energy flow logic for the HES which formed a basis for a Microsoft excel spreadsheet model applicable to the Zimbabwean electrical energy context; local weather conditions, typical peak load curves.

Hossain et al (2014) proposed an optimal power system model for a grid connected coastal area of Bangladesh endowed with RE sources for hybrid power generation. The model was simulated in the Hybrid Optimisation Model for Energy Renewable (HOMER) based on the electrical demand of the coastal area and the RE resources. In the model, the HRES was the primary energy source with grid providing the back-up power thus reducing the use of DG, hence reduction in carbon footprint. Also, the excess RE generated power would be sold to the grid.

Hove and Mushiri (2015) furthered HRES optimisation with a dimensioning of a grid integrated HES noting the poor reliability of electrical supply even to the grid connected urban areas energy consumers. The study sought to mitigate the effects of load shedding on domestic households. Their work presents a spreadsheet model which is customized to suit the scheduled electrical load shedding scenario prevailing in Zimbabwe.

In the fore-going context, this study seeks to propose a general HES model based on PV–BESS– Grid–DG which can be applied to a grid connected remote mine in rural Zimbabwe and to similar operations. The case study is backed up by DG to increase electrical energy reliability to 100%. In the model, PV-BESS will secure electrical supply, improve its reliability, reducing the running time of the DGs to reduce the operation and maintenance costs and GHG emissions.

In the model, the energy demand is primarily supplied by the PV-BESS backed up by the grid. The DG is incorporated to provide energy in extreme cases such as might be attributed to adverse weather such as storms or prolonged cloudy days and grid is absent.

2.5 PV Array Power

2.5.1 PV Array Power Output

Power output from a PV panel varies from site to site, weather conditions, time of the day as well as seasons. It is estimated from equation (2.5.1) below:

$$P_{pv} = \eta_{pv} P_{pv,ref} A, \text{ where} \quad (2.5.1)$$

$P_{pv,ref}$ = Reference Power of the PV panel, kW/m^2

η_{pv} = Panel efficiency corrected for local ambient Temperature, %

And A = Panel area, m^2

2.5.2. PV Performance dependency on ambient Temperature

PV panels work in different parts of the world and hence under different climatic conditions. As such, PV performance will be governed by the local climatic conditions and vary from site to site. It is imperative therefore, that the impact of the environmental conditions on PV performance be studied.

The panel efficiency in equation (2.5.1) above is given by Evans (1981) as follows;

$$\eta_{pv} = \eta_{ref}\,[1 - \beta(T_c - T_{ref}) + \gamma \log_{10} I_{pv}] \qquad (2.5.2)$$

η_{ref} = Panel efficiency measured at reference PV cell temperature

Efficiency is reported constant at relatively constant operating temperatures encountered with flat-plate panels, Siegel et al (1981)

T_c = PV cell temperature

T_{ref} = Reference cell temperature at which η_{ref} is determined

γ = Radiation coefficient for cell efficiency

Equation (2) above can be rewritten by subtracting and adding ambient temperature to T_c and T_{ref} above, and setting $\gamma = 0$, Siegel et al (1981), Hove (2000). Thus;

$$\eta_{pv} = \eta_{ref}\,[1 - \beta(T_c - T_a) - \beta\,(T_a - T_{ref})] \qquad (2.5.3)$$

An energy balance can be performed on a PV panel to account for incoming solar radiation , the power output of the panel and the thermal losses due to temperature gradient between panel and the ambient, thus;

$$\tau\alpha I_{pv} = \eta_{pv} I_{pv} + U_L (T_c - T_a) \quad (2.5.4)$$

where;

$\tau\alpha$ = transmittance-absorbance product of the PV panel

U_L = thermal loss coefficient per unit area between PV panel and ambient.

Efficiency in equation (2.5.3) above can be approximated to the order of 0.1 ℓα, Hove (2000). Thus equation (2.5.4) can be arranged into a temperature gradient expression as;

$$T_c - T_a = 0.9 (\tau\alpha / U_L) I_{pv} \quad (2.5.5)$$

$\tau\alpha / U_L$ can be estimated from cell temperature, ambient temperature and solar radiation measurements at nominal operating cell temperature, the NOCT conditions at which the conditions are, Stultz and Wen (1977); I_{pv} is 800W/m^2 = 2.88MJ/m^2/h, Ta = 20^{o}C, wind speed of 1m/s and $\eta = 0$

Thus $\tau\alpha / U_L$ can be determined at NOCT conditions as;

$$\text{And } \tau\alpha / U_L = (T_{c,NOCT} - T_{a,NOCT}) / I_{pv,NOCT} \quad (2.5.6)$$

Substituting equations (2.5.5) and (2.5.6) into equation (2.5.3) yields;

$$\eta_{pv} = \eta_{ref} [1 - 0.9\beta(T_{c,NOCT} - T_{a,NOCT}) I_{pv}/I_{pv,NOCT} - \beta (T_a - T_{ref})] \quad (2.5.7)$$

In equation (7) above, the parameters η_{ref}, β and T_{ref} are given as 0.12, 0.0045 and 25^{o}C respectively for Mono-Silicon PV panels, Chow (2003).

2.5.3. PV Module Power output Equations

It can thus be recalled that PV panel derived power, I_{pv}, is given in equation (2.5.1),

P_{pv} = η_{pv} $P_{pv,ref}$ A, where A is the area and η_{pv} is determined from (2.5.7)

PV panels work in different parts of the world and hence under different climatic conditions. As such, PV performance will be governed by the local climatic conditions and vary from site to site. It is imperative therefore, that the impact of the environmental conditions on PV performance be studied.

Several researchers offer different models for the prediction of PV power outputs for various climatic condition and hence geographic locations.

Rosell et al (2000) modelled power outputs in PVs for outdoor operating conditions and gave the following non-liner multi-regression equation:

$$P_{mp} = d_1 + d_2 + d_3(\ln G_T)^m + d_3(\ln G_T)^m \quad (1)$$

The coefficients d_{1-4}, m are model parameters based on the observation that PV cells are not identical.

Further work on power prediction for the PVs was carried out by Furushima et al (2006) who proposed the following relationship:

$$P = V_c I_c \left[1 - (G_T - 500)/2*10^{-4} + C_{TC}(50 - T_c)^2/4*10^{-4} \right] \quad (2)$$

Where V_c, I_c are the output voltage and current respectively

The coefficient C_{TC} = 1 if $T_c < 50$ or

= 3 if $T_c > 50$

In modeling a technical specification for a turnkey Power system, Framer (1992) investigated the impact of convective heat transfer from a PV panel. The investigation showed that with influence of wind, heat transfer and hence heat loss from the panel increased thereby reducing T_c and subsequently panel efficiency improved.

Mayer and van Dyk (2000) developed the following model based on total radiation and maximum ambient temperature:

$$P = G_T (b_1 + b_2 G_2 + b_3 T_a + b_4 V_f) \quad (3)$$

In the equation above;

V_f is the free stream local wind velocity measured 10m above the ground

b_{1-4} regression coefficients determined at solar radiation flux above 500 W/m^2

In equations (2.5.1.) and (2.5.2.) above, the cell temperature is a function of both the ambient temperature, Ta, and the nominal operating cell temperature T_{NOCT} (normally supplied by manufacturer). T_{NOCT} is defined as the cell temperature measured under open-circuit when the temperature is 20°C, at irradiance of 800W/m^2 and wind speed of 1m/s. Values are usually around 45°C. Luque and Hedegus (2003) give the linear dependence of cell temperature on ambient temperature as;

$$T_c = T_a + G_T (T_{NOCT} - 20)/800 \quad (4)$$

In this study, PV power output will be determined following the derivations from Hove (2000).

$$P_{pv} = \eta_{ref} [1 - 0.9\beta(T_{c,NOCT} - T_{a,NOCT})I_{pv}/I_{pv,NOCT} - \beta (T_a - T_{ref})] P_{pv,ref} A,$$

2.6 Solar Radiation on a Tilted Surface, PV panel

2.6.1 Angles defining the direction of beam on a tilted surface / PV panel

The sun's beam radiation on a tilted surface is illustrated in Fig 2.6.1.

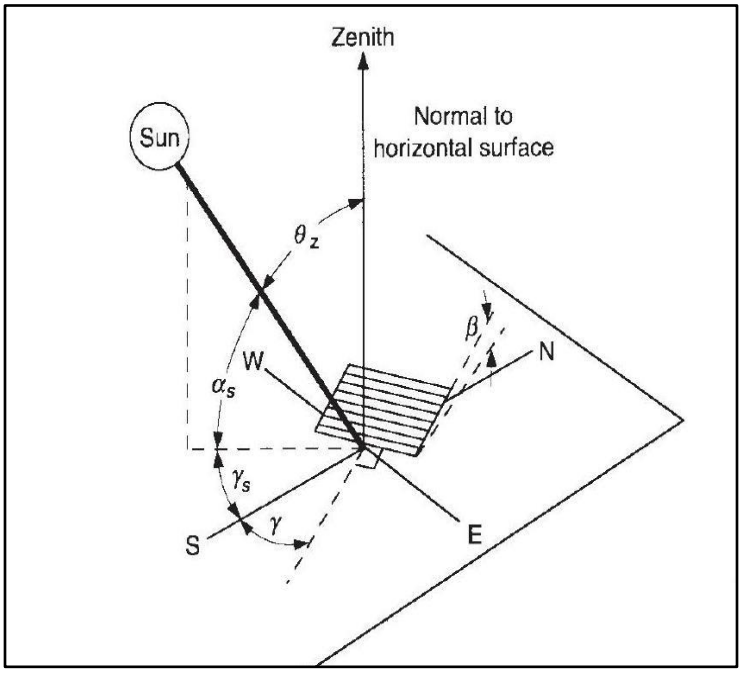

Figure 2.6.1 Sun's angles, Duffie and Beckman (2013)

Where the angles are defined as follows

δ = declination angle, angular sun's position at solar noon relative to the plane of the equator varying by day number, N, hence season.

= $23.45\sin(360/365(N+284))$; lies between $-23.45^{o} \leq \delta \leq 23.45^{o}$ (2.6.1)

φ = Latitude, location of surface (PV) north or south of the equator, lies between $-90^{o} \leq \varphi \leq 90^{o}$

θ_z = Zenith angle, the angle of incidence of beam radiation on a horizontal surface

β = Tilt of the surface measured from the horizontal, estimated at lat + 5^{o}, approximately 22^{o} for the case study

γ = Surface azimuth angle; displacement of the projection on a horizontal plane of the normal to the surface from the local meridian. For a surface in southern hemisphere facing north, $\gamma = 180^{o}$

ω = hour angle, the angular displacement of the sun from the local meridian due to rotation of the earth on its axis at 15^{o} per hour.

= $\omega = 15\ (t - 12)$, where 't' is the local time in hours (2.6.2)

2.6.2 Angle of beam radiation on tilted surface

The angle of incidence of a beam radiation on a tilted surface is given by Duffie and Beckman (2013), equation (2.6.3). It is defined as the angle between beam radiation on a surface and the normal to the surface.

$$\cos\theta = \sin\delta\sin\varphi\cos\beta - \sin\delta\cos\varphi\sin\beta\cos\gamma + \cos\delta\cos\varphi\cos\beta\cos\omega + \cos\delta\sin\varphi\sin\beta\cos\gamma\cos\omega + \cos\delta\sin\beta\sin\gamma\sin\omega \quad (2.6.3)$$

In this study, for the case study being located in the southern hemisphere, it is assumed that collector at tilt β is North facing hence azimuth is 180^o. Equation (2.6.3) then reduces to

$$\cos\theta = \sin\delta\sin\varphi\cos\beta + \sin\delta\sin\beta\cos\varphi + \cos\delta\cos\varphi\cos\beta\cos\omega - \cos\delta\sin\varphi\sin\beta\cos\omega \quad (2.6.4)$$

$$= \sin\delta(\sin\varphi\cos\beta + \cos\varphi\sin\beta) + \cos\delta\cos\omega(\cos\varphi\cos\beta - \sin\varphi\sin\beta)$$

Equation (2.6.4) can be compared to the example of special trigonometric properties given below;

$$\sin(A + B) = \sin A\cos B + \cos A\sin B$$

$$\cos(A \pm B) = \cos A\cos B \mp \sin A\sin B$$

Thus equation (2.6.4) simplifies to;

$$\cos\theta = \sin\delta\sin(\varphi + \beta) + \cos\delta\cos\omega\cos(\varphi + \beta) \quad (2.6.5)$$

2.6.3 Angle of beam radiation on a horizontal surface

In this study, the case study is located in the southern hemisphere and the collector is facing north. Surface azimuth is 180^o and the tilt β for a horizontal collector is 0^o. The angle of incidence, cosθ, is then defined as the zenith angle of the sun, θ_z. the Equations 2.6.3 or 2.6.5 then reduce to;

$$\cos\theta_z = \sin\delta\sin\varphi + \cos\delta\cos\omega\cos\varphi \quad (2.6.6)$$

2.6.4 Ratio of beam radiation on a tilted surface to that on a horizontal surface

Solar radiation data is normally available for horizontal surfaces. In dimensioning of PV arrays for electricity generation, PV panels are always tilted (when not tracked) at angles comparable to the latitude for maximum solar radiation. To estimate solar radiation on these tilted surfaces, a geometric ratio, R_b, is used. The ratio relates the beam on a tilted surface to that on a horizontal surface, Duffie and Beckman (2013). Therefore, with a knowledge of the ratio, radiation on a tilted surface can be estimated. R_b can be derived with the aid of the following diagram Fig 2.6.2.

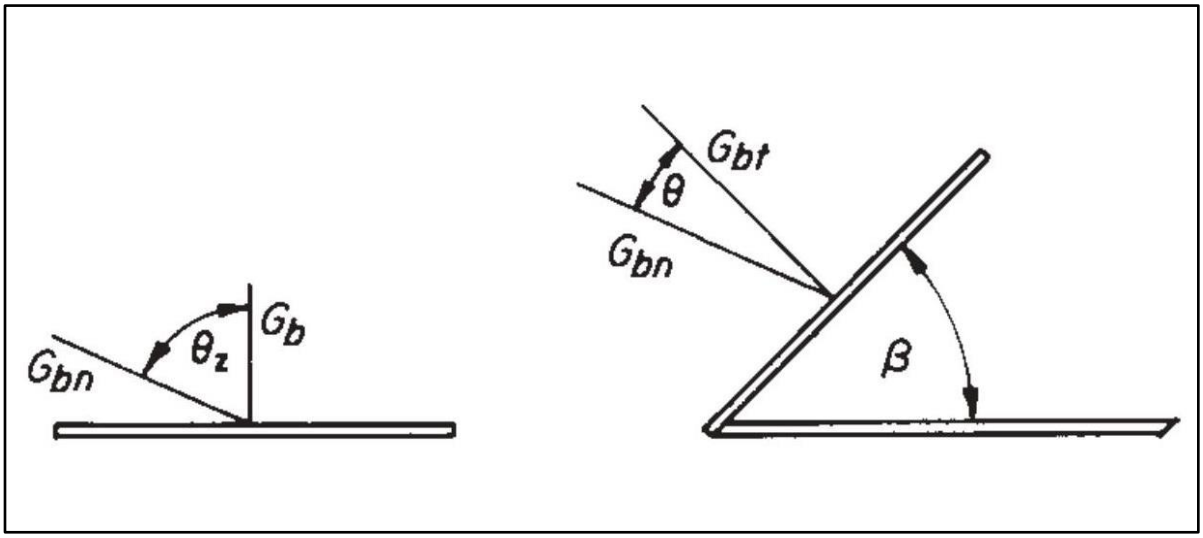

Figure 2.6.2 Radiation on a horizontal and tilted surfaces, Duffie and Beckman (2013)

From Fig 2.6.2, On the horizontal surface, incident radiation, G_b is estimated as $G_{bn}\cos\theta_z$. Similarly on a tilted surface, G_{bt} is estimated from $G_{bn}\cos\theta$.

The ratio of the beam; tilted to horizontal is found by

$R_b = G_{bt} / G_b$

$= G_{bn}\cos\theta / G_{bn}\cos\theta_z$

$= \cos\theta / \cos\theta_z$ (2.6.7)

Thus, equation 2.6.7 can be solved with equations 2.6.5 and 2.6.6 as follows;

$R_b = \cos\theta / \cos\theta_z$

$= \frac{\sin\delta\sin(\varphi + \beta) + \cos\delta\cos\omega\cos(\varphi + \beta)}{\sin\delta\sin\varphi + \cos\delta\cos\omega\cos\varphi}$ (2.6.8)

2.6.5 Radiation on a tilted surface

- In the preceding sub-sections, the angles defining the sun's position and the surface were given; latitude – φ, surface tilt – β, surface azimuth – γ and hence calculation of the declination δ and the hour angle ω and for each day of the year using 2.6.1 and 2.6.2 respectively

- With these angles, R_b, can be calculated using equation 2.6.8 for each hour

- Diffuse radiation fraction on a horizontal surface is obtained from equation 2.6.9 below as;

  $I_d = K_{gr} * I_o$ (2.6.9)

- Total beam radiation on a horizontal surface is obtained from the subtracting the diffuse fraction from the total radiation on the horizontal surface;

  $I_{bh} = I_o – I_d$; i.e.

  $I_{bh} = I_o - K_{gr} * I_o$ (2.6.10)

- Beam radiation on a tilted surface, I_{bt}, is calculated from R_b and the beam radiation on a horizontal surface.
- $I_{bt} = R_b * I_{bh}$ or $I_{bh} * \frac{\cos\theta}{\cos\theta z}$ (2.6.11)

- Finally, the total hourly radiation on a tilted surface will be obtained as

$$I_{coll} = I_d + I_{bt}$$

$$= K_{gr} I_o + (I_o - K_{gr} I_o) \frac{\cos\theta}{\cos\theta z} \text{ or } I_o(K_{gr} + (1 - K_{gr}) \frac{\cos\theta}{\cos\theta z}) \quad (2.6.11)$$

The above simplification assumes diffuse radiation and the ground-reflected radiation to be isotropic regardless of surface orientation, Hottel and Woertz (1942), hence total radiation on a tilted surface is $I_{bh}R_b$ + Id. However, the work of Lui and Jordan (1963) shows the influence of another component on diffuse radiation - the surrounding's diffuse reflectance.

2.7 Selection of the Battery Energy Storage System (BESS)

In this section, the author gives a general overview of the available technology in the market. Nevertheless, lead-acid batteries were selected in the model development due to its dominance in application.

2.7.1 Battery Energy Storage

Energy Storage can supply more flexibility and balancing to the grid, providing a back-up to intermittent renewable energy and enhance the reduction or elimination of the carbon footprint in electricity supply, improve the security of energy supply promote price stabilization of electrical energy supply. In their Working Paper "The future role and challenges of Energy Storage", January 2013, European Commission noted that BESS are installed in capacity of 100GW. The

IEA has projected that the application of BESS in the world in 2050 will be an increase of between 189GW and 305GW, in relation to an output of REs of 15% to 30%.

BESS find wide applications range anywhere from 5 kWh to 50 MWh and distinct fast response, mobility and can be integrated in high power or high energy applications. BESS can be applied for peak shaving and time of use cost management. Some of the applications of BESS include:

- **Peak shaving in low voltage grid** *Typical duration is 2 hours, with 1 to 2 cycles per day*

  BESS can store excess energy in periods of low demand and release it in periods of high demand. In this application, peak demand is reduced and consequently the energy cost for 'maximum-demand' customers.

- **Integration of renewable energy into the grid** *Numerous small cycles per day*

BESS can address the intermittence in REs electricity generation by shaving off renewable peak generation in times of high production, for example during the noon by PVs, and low demand and release it when the grid is off (through scheduled load shedding or maintenance) or during periods of low or no production by REs.

2.7.2 Common Types of Battery

This study focused on two main types that have gained wide applications in the RE industry – the lead acid and the lithium ion batteries.

2.7.2.1 Lead-based Batteries

Lead-based batteries technology has over 100 years of application in the automotive industry and industrial applications. They are well-integrated in several on-grid applications for grid operators and end-users. It is estimated that approximately 80% of the total installed capacity of industrial batteries in both mobile and stationary applications is lead-acid based. Lead-based batteries are available in mainly two different types of - flooded or vented Lead-acid batteries requiring maintenance amd the maintenance-free valve-regulated Lead-acid (VRLA) batteries.

Typical performance characteristics for Lead-acid based on –grid BESS:

• Capacity – 1 Ah up to 16,000 Ah

• Energy density – 25-50 Wh/kg, (60-40 Wh/l)

• Energy Efficiency – approximately 85%

• Calendar life – up to 20 years

• Cycle life - >2,000 cycles based on 80% DOD

• Operation temperature range - 30°C up to +50°C

Advantages of Lead acid batteries

- They are robust and can be used in various application conditions.
- They can be integrated into large battery arrangements with simple management systems.
- They are cheaper than other battery technologies; typical about 120 to 200 € to install
- Their running cost per kWh electricity throughput is cheap at values of 0.1 to 0.15€ per kWh turn over for battery only.
- Lead-based batteries are recyclable

For grid applications, advanced Lead based batteries (for example AGM or enhanced flooded and VRLA batteries) continue to be developed in order to provide increased cycle life, charge acceptance, discharge performance, and cost reduction. Their specific power will be improved with advanced additives to the active materials and lower internal resistance designs; while cycle life will be lengthened through design enhancements such as corrosion-resistant Lead alloy materials and a more intelligent battery operation mode.

2.7.2.2 Lithium-based Batteries

The commercialisation of Lithium-Ion batteries (Li-ion) began in the 1990s with applications in the small portable market. Application in industrial markets started in 2000 with success. Li-ion batteries are superior to the lead-acid batteries as given in their main characteristics below;

- High energy density (150-200 kWh/m^3, 140 kWh/ton at battery level)
- High efficiency, approximately 100%
- Long cycle life (>5,000 cycles @ 80% depth of discharge)
- Long calendar life of more than 20 years
- Li-ion batteries are maintenance-free
- Are scalable, can be adapted to practically any voltage, power and energy requirement
- State of charge and State of health indication

Whilst Li-ion batteries require sophisticated electronics for control, they offer accurate management and control. Their use in stationary applications started in 2010 in electric vehicles, EVs. It is estimated that about 100MW of stationary Li-ion batteries are operating in grid connected installations worldwide including in RE generators in capacities of kW to MW. EUROBAT reported that recycling processes and installations are in place achieving a recycling efficiency well above 50%.

2.7.3 Modelling of the BESS

2.7.3.1 Modelling Battery Life

Battery life as applied to HRES is dependent on temperature, charging strategy among other factors but more importantly, battery life is affected by the rate of discharge and depth of discharge, Drouilhet and Johnson (1997) and hence life of batteries is affected when charged by intermittent energy generators such as PV. A prediction method was offered where the charge life, CH_R is given as;

$$CH_R = L_R DOD_R C_R \quad (2.7.1)$$

L_R = Battery cycle life at rated DOD_R and discharge current I_R

DOD_R = Depth of discharge at which cycle life was determined

C_R = Rated Amp-hour capacity at rated discharge current, I_R

In real operation, the charge life a of the cell CH_a will always be less than CH_R when the battery is cycled more deeply than the reference DOD_R and will be greater than CH_R when the battery is cycled less deeply, Symons (1995). Battery charge life utilized with each discharge in the operating life can be adjusted according to the actual depth of discharge and discharge rates. Effective Amp-hour discharge is introduced and is defined as

$$d_{eff} = d_{act} \times f_{DOD} \times f_1 \qquad (2.7.2)$$

Scaling factors f_{DOD} and f_1 are defined as follows;

f_{DOD} accounts for the effect of DOD on battery charge life utilized and is obtained from a best fit curve from the manufacturer's cycle life versus DOD charts.

f_1 accounts for the effect of rate of discharge on battery charge life utilized and is obtained from a best fit curve of actual Amp-hour capacity versus actual discharge current based on manufacturer's Amp-discharge data.

In this study, the scaling factors are defined as follows;

$$f_{DOD} = 1.358(DOD_A / DOD_R)^{-1.014} \qquad (2.7.3)$$

$$f_1 = 0.923\ (B_{disch} / B_{cap})^{-0.127} \qquad (2.7.4)$$

By definition, a battery will reach its rated life if the cumulative sum of the effective discharges reaches its useful life. However, physical factors prevent the realization of such an ideal situation, for example corrosion of plates, contamination of battery electrolyte.

Cycle life of the battery is estimated using the equation below by summing up the effective discharges estimated from equation 2.7.2 above.

2.8. Diesel Generators Selection

2.8.1 Diesel Power Output

Sizing of the DG is normally done by selecting a DG unit which matches the peak load requirements of the application. The DG operates most efficiently when running between 80-90% of its rated power and become less and less efficient as the load decreases according to Nafeh (2010) when its specific fuel consumption increases. The DG rated power Q_{DG} is normally designed to be at least equal to the peak load demand, Nafeh (2010).

The specific fuel consumption of the DG at no load is high. Kaldellis (2007) further states that operation of the DG below 30% of full load for long periods should be avoided in order to avoid serious maintenance problems, like chemical corrosion and glazing which occur due to wet stacking. Wet stacking is defined as the occurrence of unburnt diesel or carbon in the exhaust system of the DG because the operating temperature is not high enough to combust the diesel. Wet stacking results in corrosion of the exhaust system, affect the pistons, build up in the exhaust side of the engine, resulting in fouled injectors and a buildup of carbon on the exhaust valves, turbo charger and exhaust.

Excessive deposits can result in a loss of engine performance as gases bypass valve seatings, exhaust buildup produces back pressure, and deposits on the turbo blades reduces turbo efficiency. Permanent damage will not be incurred over short periods, but over longer periods, deposits will scar and erode key engine surfaces. Also, when engines run below the designed operational temperature, the piston rings do not expand sufficiently to adequately seal the space between the pistons and the cylinder walls. This results in unburned fuel and gases escaping into the oil pan and diluting the lubricating properties of the oil, leading to premature engine wear, Appendix 3.

The status of the DG in any hour is either on or off depending with a power output of the DG rated power or zero respectively. The DGs have a possibility to be operated in two energy dispatch strategies, Hove and Tazvinga (2012);

- Dispatched in the night when there is no generation by the PV. In this case manual operation of the DG is possible without sophisticated control systems. In this dispatch

strategy, power might be wasted and might shorten DG life requiring frequent maintenance due to wet stacking if the load is below 30% of the rated DG power, Kaldellis (2007).

DG Output = Q_{DG} when $\omega \geq \omega_s$ (2.8.1)

= 0 when $\omega \leq \omega_s$ (2.8.2)

Or DG Output = if ($\omega \geq \omega_s$, Q_{DG},0) in a spreadsheet

- Load following strategy - The DG is to be switched on when the load reaches a minimum threshold as a percentage of the DG rated power, example when load is 30%. This strategy ensures optimum operation of the DG at likely high load factors, prolongs the DG service life, reduces maintenance costs and lowers specific fuel consumption. Capital costs plus the maintenance costs will be incurred for the required control systems.

  Let the threshold load be d_{ON}.

DG Output = Q_{DG}, when Load, $L_h \geq d_{ON}$

= 0, when Load, $L_h < d_{ON}$

= if ($L_h \geq d_{ON}$, Q_{DG},0) in a spreadsheet

The DG is normally sized as the peak load. Therefore, the value d_{ON} can be defined as any value up to Peak Load (QDG). Thus

d_{ON} = $0.3Q_{DG} \leq d_{ON} \leq Q_{DG}$ (2.8.3)

As the value of d_{ON} approaches QDG, the operational hours of the DG get lower hence increasing the lifetime of the DG while reducing the O and M costs.

2.8.2 Diesel Fuel Consumption

The diesel fuel consumption in a given hour is modelled Dufo-Lopez and Bernal-Agustin (2008)

$$F = F_o Q_{DQ} + F_1 Q_{gen} \quad (2.8.4)$$

Where F_o = Fuel consumption at no Load, it is intercept divided by Q_{DG}, rated power

Q_{gen} = Generator power output

F_1 = generator fuel curve slope, $L/hr/kW_{output}$

Generally, for the diesel generator; F_o is 0.0845 L/h/kW and F_1 0.246 L/h/kW, i.e.

Generator Operational Life

$$= \frac{\text{Generator Liftetime,hours}}{\text{Annual run hours}}$$

Scheduled Maintenance Stage	Generator Running hours
Routine Planned Maintenance	500
Major Maintenance	6,000
Replacement	15,000

Table 2.8.1 Typical DG Maintenance Schedule, Hove and Tazvinga (2012)

2.8.2 Estimation of the Direct Green House Gases Emissions from DGs

Due to the combustion of diesel oil, a fossil fuel, in the generation of back up electricity, GHG (CO_2, CH_4, and N_2O) are released. The GHG quantities are estimated from the quantity of the fuel consumed as well as from emission factors as given in the IPCC Guidelines on GHG Emissions (IPCC 2006). The Tier 1 method is used and is based on the fuel consumed and the default emission factor in the absence of the country specific emission factor.

In this study, the fuel consumption is not directly measured. The diesel oil consumed can be estimated from the load satisfied by DG factored by the Net Heat value of the diesel oil and diesel generator efficiency, assumed at 40%. The procedure assumes complete combustion. Alternatively, the load demand is divided by the period (in hours) without grid to give average load in kW. The average load in kW is then factored into the general diesel equation Equation 2.84. The third approximation procedure is given by Hove (2000). In his work, Hove (2000) gives the specific fuel consumption at 0.35 L/kWh. Of the three methods, the second and Hove's approximate consumption give closer estimations at about 9.4% variance. Hove's approach being the conservative approach will be used in the estimations in this study.

$$Emission_{GHG,Diesel} = \text{Fuel Consumption} \times \text{Emission Factor}_{GHG,\ diesel\ fuel} \quad (2.8.5)$$

Typical values of emission factors for diesel oil are given in the table below.

Greenhouse Gas	**Emission Factor** Kg GHG / TJ Fuel
CO_2	74 100
CH_4	3
N_2O	0.6

Table 2.8.2 Default emission factors for Stationary Combustion in the Energy Industries, IPCC (2006)

The NHV of diesel oil is given as 45 MJ/kg (39MJ/L diesel oil), www.world-nuclear.org

Chapter 3 Methodology

3.1 Project Methodology Flow

To achieve the objectives set in the study, data collection methods were applied and procedures for evaluations of model results explored. The actual steps taken in achieving the objectives are given in this chapter.

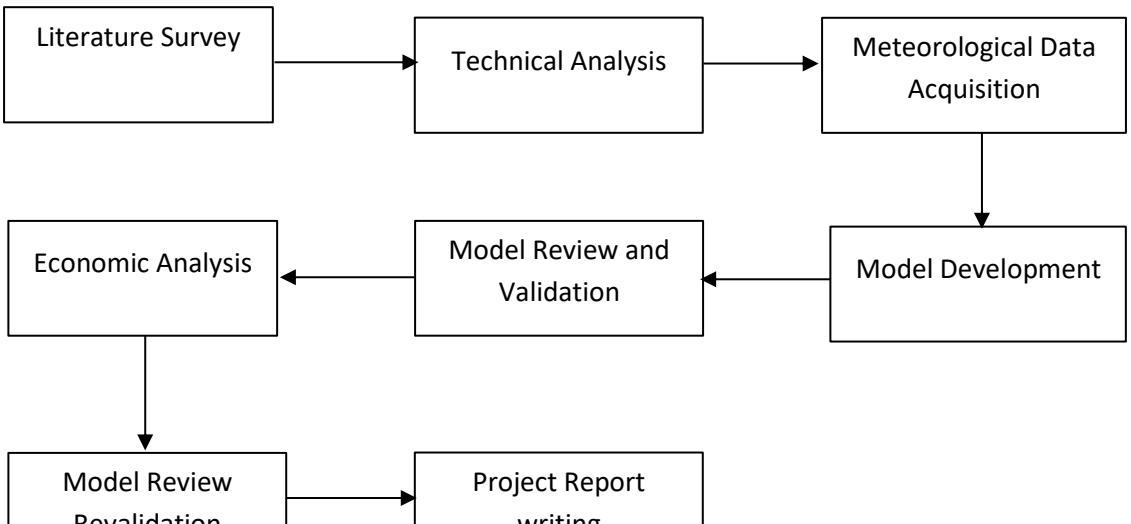

Fig 3.1 Methodology Flowchart, Muguti (2009)

3.2 Technical Analysis

The model was developed based on available radiation, panel efficiencies at prevailing ambient temperatures, technical specifications of panel as given by the PV vendor, efficiencies and voltage limitations of the inverter and the battery storage.

3.3 Solar Radiation Data Acquisition

3.3.1 Solar Radiation Data

As mentioned in Section 3.1, the PV output performance is a function of the solar radiation that is collected on the panel.

In this study, hourly solar radiation collected a horizontal plane was accessed from **So**lar Radiation **Da**tabase for the year 2005, www.soda-pro.com. The solar radiation data (radiation and clearness index) for this study were obtained from satellite measurements for 2005. Later data from 2006 onwards was for sale. Also, the site-specific long-term data is not available. The ground data could not be measured in this study due to lack of adequate time and also the prohibitive

cost and resources to execute the measurements. The data was cleaned to remove some error values of the order 999,999.

Source	**HelioClim-3 Database of Solar Irradiance v5 (derived from satellite**
Provider	MINES ParisTech / Armines / Transvalor (France)
website	http://www.soda-is.com
Date Accessed	28 April 2017
Data Collected	Sky Hourly radiation, Clearness Index
Site Name	Ruia Mine, Mount Darwin, Zimbabwe
Site latitude	-16.75
Site longitude	31.45
Elevation	968 m
Date Beginning	01 – 01 - 2005
Date Ending	31 – 12 -2005
Time Reference	Solar Time, TST
Period of Integration	hour

Table 3.3.1 Solar radiation Data Summary of Acquisition

This data was therefore modelled using some correlations to approximate solar radiation on the ground for the site. As first step, correlation coefficients derived by Hove et al (2014) for Zimbabwe were applied to approximate satellite clearness index to the ground clearness index using Duffie and Beckman (2013)\s clearness transformation;

$$K_{gr} = a + bK_{sat} \quad (3.3.1)$$

For the location; latitude -16.75 and Longitude 31.45, a and b constants are given as 0.227 and 0.681 respectively, Hove et al (2014).

Ksat is also calculated from the satellite measured irradiation as a ratio of

The Diffuse radiation on a horizontal surface as related to the hourly radiation is given from The Orgill and Hollands (1974) diffuse ratio correlation and the clearness index as below:

$$I_d / I_o = K_{gr}, \text{ where} \quad (3.3.2.)$$

$$K_{gr} = 1 - 0.249*K_{gr}, \text{ for } 0 \leq K_{gr} \leq 0.35$$

$$K_{gr} = 1.557 - 1.84*K_{gr}, \text{ for } 0.35 \leq K_{gr} \leq 0.75$$

$$K_{gr} = 0.77, \text{ for } K_{gr} > 0.75$$

The diffuse radiation can be calculated by rearranging equation 3.2.2 as

$$I_d = K_{gr}* I_o \quad (3.3.3)$$

3.3.2 Site Ambient Temperature Data

Source	**Modern-Era Retrospective Analysis for Research and Applications (MERRA)**
Provider	National Aeronautics and Space Administration (NASA) / Goddard Space Flight Center

Website for more information	http://gmao.gsfc.nasa.gov/reanalysis/MERRA-2
Date Accessed	06 May 2017
Data Collected	Ambient Temperature
Site Name	Ruia Mine, Mount Darwin, Zimbabwe
Site latitude	-16.75
Site longitude	31.45
Elevation	968 m
Date Beginning	01 – 01 - 2005
Date Ending	31 – 12 -2005
Time Reference	Solar Time, TST
Period of Integration	hour

Table 3.3.2 Ambient temperature data - Summary of Acquisition

3.4 Site Energy Demand Profile and Load Shedding Programme

3.4.1 Site Energy Demand Profile

Ruia Gold Mine in Mount Darwin, Mashonaland Central Province of Zimbabwe was chosen as case study in this research. The site lies 16.75^{o} latitude South and 31.45^{o} East, longitude. An electrical energy consumption survey was carried out on site. The electrical consumers included process pumps, smelter heaters, computers, lighting (in offices, camp accommodation and street lighting), electric stove in the kitchen, refrigerator, freezer, CCTV and WiFi Router. The electrical demand is supplied from the grid and in the case of power outage (more commonly referred to as load shedding) by four DGs with a total power rating of 360 kVA (100 kVA Cummins, 180 kVA Perkins, 50 kVA Deutz and 30 kVA Perkins).

In a day, the typical energy consumption is about 4,384.319kWh with a peak load of 197.543kW. As the mine is expand, it is foreseen to increase site accommodation and add extra consumers such as extra lighting, electric geysers, air conditioners and two extra pumps for the foreseen heap leaching process. In this scenario, the daily energy consumption would be 5,989.781 kWh ≈6,000kWh with a peak load of 278.283 kW.

In general, for load management, the writer proposes to remove the air conditioning, electric stove and geysers from the list of consumers to reduce the size of the PV array and or BESS. Various solar thermal technologies can be applied to supply the electrical needs; solar water heating, space heating and cooling and solar water pumping, Kalogirou (2004). The remaining electrical consumers, in this scenario, would account on a daily basis for 4,276.739 kWh of electrical energy with a peak load of 184.783 kWh.

In this study, the model is based on the load 'as is' profile of 4.38MWh.

3.4.2 Load Shedding Programme

Load shedding or power outage is when there no electrical supply by the utility as scheduled and communicated from time to time. It is the scheduled and controlled temporary way of disconnecting power to some parts of grid-connected consumer areas when there is not enough electricity to meet the needs of the customers. This is as a result of a shortage of capacity and a high demand for electricity, especially in the winter season when demand is increased. Load shedding does not include outage due to faults nor planned maintenance.

The schedule affecting the case study is as per the ZETDC schedule for the Northern Region, Bindura District, Mount Darwin area as officially communicated on August 14, 2014, www.zetdc.co.zw (2014). The schedule is given in Table 3.1

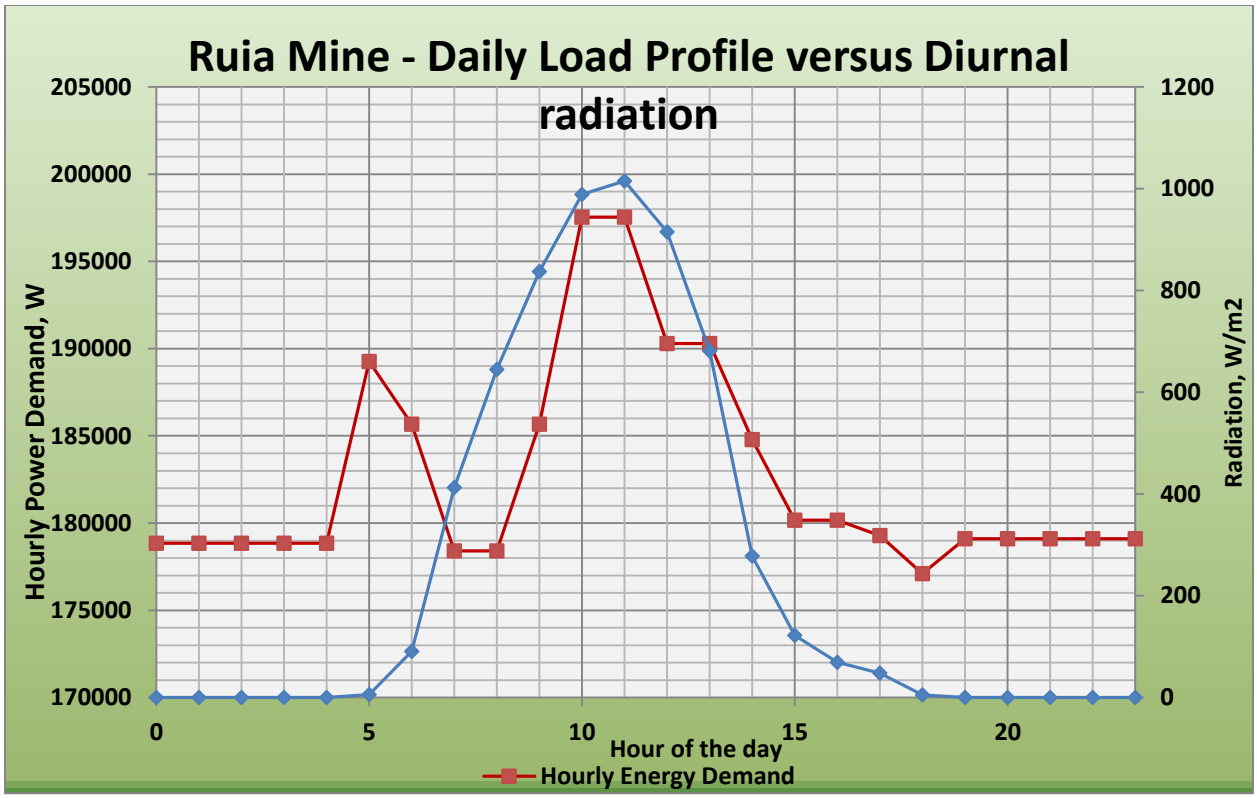

Fig 3.2 Hourly Energy Demand Profile for Ruia Mine

Time	Air conditioning	Air conditioning	Boiler 1	Boiler 2	Carbon column pump 1	Carbon column pump 2	CCTV Data capturing	Communication Radio	DSTV Decoder	Electric Stove 1	Freezer - Capri	Geysers	Heap leaching Pump motor	Heat element smelter 1	Heat element smelter 2	Heat element smelter 3	IT Server	Laptop HP	Laptop Lenovo	Leaving Room TV	Light bulb type 1	Light bulb type 2	Light bulb type 3	Light bulb type 4	Light bulb type 5	Light bulb type 6	Light bulb type 7	Printer type 1	Radio	Refrigerator – Hi Sense	Water cooler	Water Pump motor	WiFi Antenna	WiFi Booster	Hourly Energy Demand	Hourly Load / Day
0	0	0	1	1	1	1	1	0	0	0	0.25	0	1	0	0	0	0	0	0	0	1	1	1	0	0	1	1	0	0	0.25	0	0	0	0	178852	0.0408
1	0	0	1	1	1	1	1	0	0	0	0.25	0	1	0	0	0	0	0	0	0	1	1	1	0	0	1	1	0	0	0.25	0	0	0	0	178852	0.0408
2	0	0	1	1	1	1	1	0	0	0	0.25	0	1	0	0	0	0	0	0	0	1	1	1	0	0	1	1	0	0	0.25	0	0	0	0	178852	0.0408
3	0	0	1	1	1	1	1	0	0	0	0.25	0	1	0	0	0	0	0	0	0	1	1	1	0	0	1	1	0	0	0.25	0	0	0	0	178852	0.0408
4	0	0	1	1	1	1	1	0	0	0	0.25	0	1	0	0	0	0	0	0	0	1	1	1	0	0	1	1	0	0	0.25	0	0	0	0	178852	0.0408
5	0	0	1	1	1	1	1	0	0	1	0.25	0	1	0	0	0	0	0	0	0	1	1	0	0	0	1	1	0	0	0.25	0	1	0	0	189260	0.0432
6	0	0	1	1	1	1	1	0	0	1	0.25	0	1	0	0	0	0	0.25	0.25	0	1	0	0	0	1	0	1	1	0	0.25	0	1	0	0	185663	0.0423
7	0	0	1	1	1	1	1	0	0	0	0.25	0	1	0	0	0	0	0.25	0.25	0	1	0	0	0	1	0	1	1	0	0.25	0	1	0	0	178403	0.0407
8	0	0	1	1	1	1	1	0	0	0	0.25	0	1	0	0	0	0	0.25	0.25	0	1	0	0	0	1	0	1	1	0	0.25	0	1	0	0	178403	0.0407
9	0	0	1	1	1	1	1	0	0	1	0.25	0	1	0	0	0	0	0.25	0.25	0	1	0	0	0	1	0	1	1	0	0.25	0	1	0	0	185663	0.0423
10	0	0	1	1	1	1	1	0	0	1	0.25	0	1	1	1	1	0	0.25	0.25	0	1	0	0	0	1	0	1	1	0	0.25	0	1	0	0	197543	0.0451
11	0	0	1	1	1	1	1	0	0	1	0.25	0	1	1	1	1	0	0.25	0.25	0	1	0	0	0	1	0	1	1	0	0.25	0	1	0	0	197543	0.0451
12	0	0	1	1	1	1	1	0	0	0	0.25	0	1	1	1	1	0	0.25	0.25	0	1	0	0	0	1	0	1	1	0	0.25	0	1	0	0	190283	0.0434
13	0	0	1	1	1	1	1	0	0	0	0.25	0	1	1	1	1	0	0.25	0.25	0	1	0	0	0	1	0	1	1	0	0.25	0	1	0	0	190283	0.0434
14	0	0	1	1	1	1	1	0	0	0	0.25	0	1	1	1	1	0	0.25	0.25	0	1	0	0	0	1	0	1	1	0	0.25	0	0	0	0	184783	0.0421
15	0	0	1	1	1	1	1	0	0	1	0.25	0	1	0	0	0	0	0.25	0.25	0	1	0	0	0	1	0	1	1	0	0.25	0	0	0	0	180163	0.0411
16	0	0	1	1	1	1	1	0	0	1	0.25	0	1	0	0	0	0	0.25	0.25	0	1	0	0	0	1	0	1	1	0	0.25	0	0	0	0	180163	0.0411
17	0	0	1	1	1	1	1	0	0	1	0.25	0	1	0	0	0	0	0.25	0.25	0	1	0	0	0	1	0	1	0	0	0.25	0	0	0	0	179283	0.0409
18	0	0	1	1	1	1	1	0	0	0	0.25	0	1	0	0	0	0	0.25	0.25	0	1	1	0	1	1	1	1	0	0	0.25	0	0	0	0	177104	0.0404
19	0	0	1	1	1	1	1	0	0	0	0.25	0	1	0	0	0	0	0	0	0	1	1	1	1	0	1	1	0	0	0.25	0	0	0	0	179105	0.0409
20	0	0	1	1	1	1	1	0	0	0	0.25	0	1	0	0	0	0	0	0	0	1	1	1	1	0	1	1	0	0	0.25	0	0	0	0	179105	0.0409
21	0	0	1	1	1	1	1	0	0	0	0.25	0	1	0	0	0	0	0	0	0	1	1	1	1	0	1	1	0	0	0.25	0	0	0	0	179105	0.0409
22	0	0	1	1	1	1	1	0	0	0	0.25	0	1	0	0	0	0	0	0	0	1	1	1	1	0	1	1	0	0	0.25	0	0	0	0	179105	0.0409
23	0	0	1	1	1	1	1	0	0	0	0.25	0	1	0	0	0	0	0	0	0	1	1	1	1	0	1	1	0	0	0.25	0	0	0	0	179105	0.0409
																																			4384319	**1.0000**

Table 3.4.1., Daily Hourly Energy Load, Ruia Mine

Day	Time	1	2	3	4	5	6	7	8	9	10	11	12	13	14	15	16	17	18	19	20	21	22	23	24
Monday																									
Tuesday																									
Wednesday																									
Thursday																									
Friday																									
Saturday																									
Sunday																									

Table 3.4.2 Load Shedding Program for ZETDC Northern Region, Bindura District

3.5 The PV – BESS – Grid – DG System

3.5.1 PV sizing methods

Previous research work has identified 3 main methods for the sizing of PV and battery arrays;

- Intuitive method
- Numerical method
- Analytical Method

3.5.1.1 Intuitive Method

In this method, the daily energy demand load is estimated and Peak Sun Hours estimated for a year, normally taken from the period of least radiation such as in winter. From these, the PV power can be estimated as given below;

$$P_{pv} = E_L / \eta_s \eta_{inv} PSH \quad (3.5.1)$$

And the battery capacity can be estimated as follows;

$$C_{wh} = E_L * DOA / V_B \eta_B DOD, \quad (3.5.2)$$

DOA are number of days of autonomy, the period when the PV system will be able to provide electrical power. DOD is the permissible depth of discharge of the battery and V_B and η_B are the battery voltage and the efficiency respectively,

The above methods, though simple, can result in an under design or over design, Khatib et al (2013).

3.5.1.2 Numerical Methods

These are system simulation methods where for each time period, an hour or day, a system energy balance is calculated. The methods are considered more accurate and concept such as energy reliability can be applied as a constraint. Loss of Load Probability (LLP) and other related parameters are also included in the simulations. LLP is defined as the probability that a load's power requirement will not be made. Sidrach-de-Cardon and Lopez (1999) presented a numerical method on a qualitative model for sizing stand-alone photovoltaic systems. The proposed model could be used with the same accuracy for other locations.

3.5.2 Method Applied in this Research

The numerical method will be used where for a defined load and solar radiation profile, the main variables governing the energy performance of the HRES are the PV array size (A/A_o), DG rated Power (P-DG), battery capacity (B_{cap}/L_{day}) and the strategy for DG operation, Hove and Tazvinga (2012).

3.5.3 The PV – BESS – Grid – DG System Configuration

.

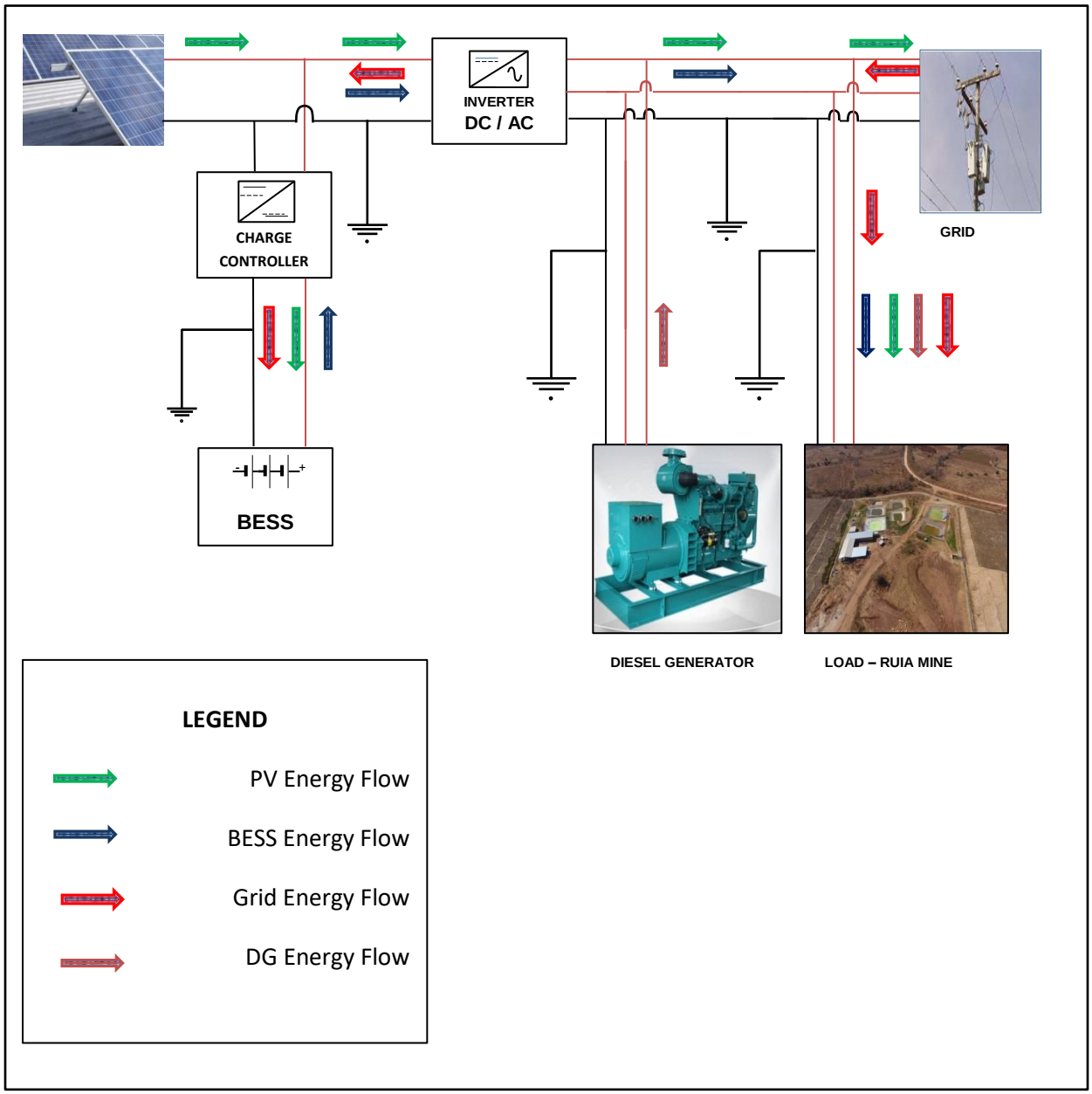

Fig 3.3 PV-BESS-Grid-DG System Configuration

3.5.4 The PV – BESS – Grid – DG System Configuration Energy Flow Logic

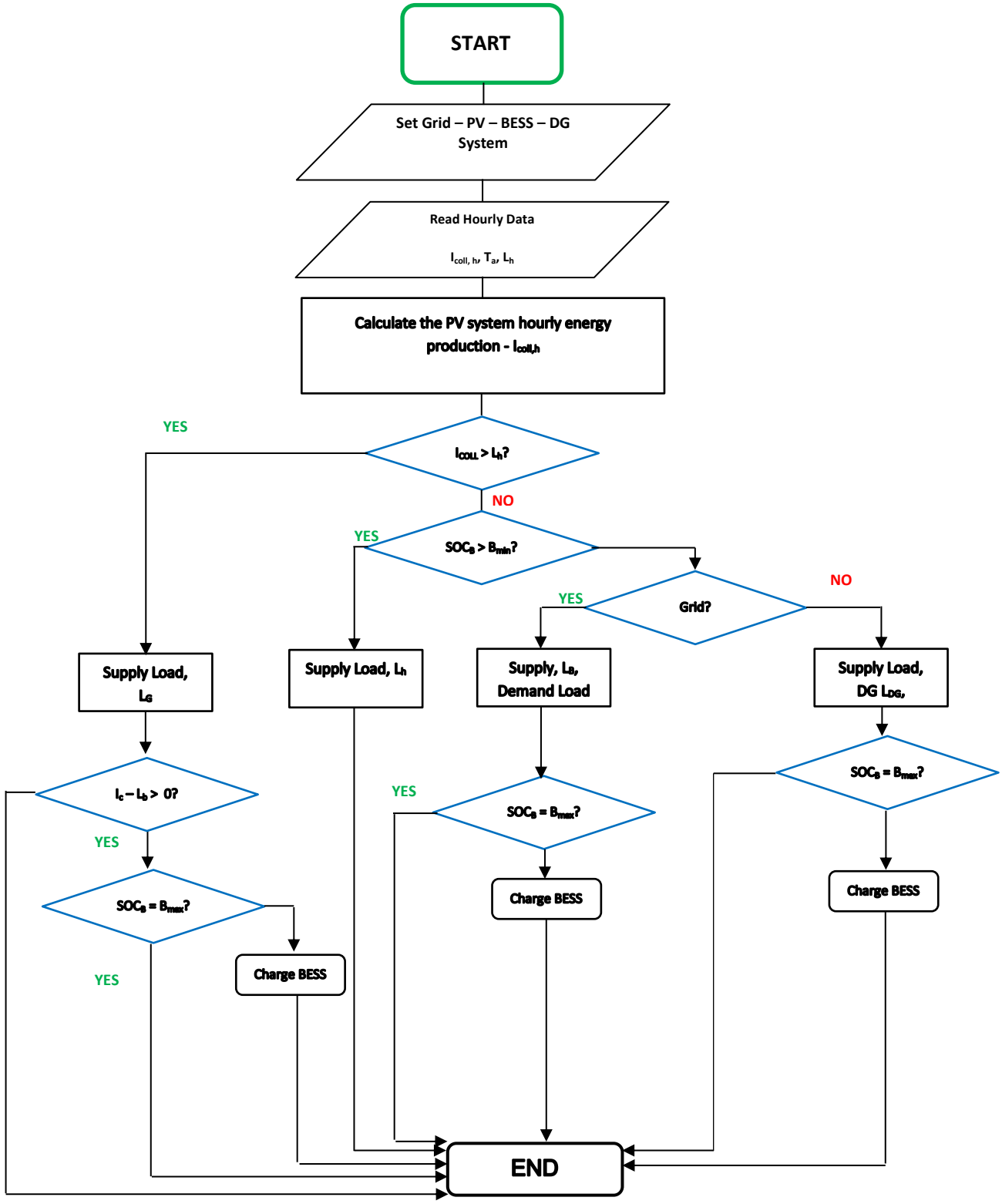

Fig 3.4 The PV – BESS – Grid – DG System Configuration Energy Flow Logic

3.5.5 The PV – BESS – Grid – DG System Description

The power control logic is shown in the fore-going figure. The main supply is the PV with the BESS. The grid provides the back-up power that would normally have been provided by the DG. The DG's function in this architecture has been reduced to only provide limited power in the absence of the power from the grid, inadequate or no power from the PV and inadequate or no power from the BESS so as to minimize energy cost and reduce greenhouse gas emissions. The author proposes that the grid is used for back-up power only so as to model a system with 100% energy reliability and increase penetration of renewable energy.

Level 1

The PV provides power through generated power Ppv. When P_{pv} is higher than the load factored with inverter efficiency, $P_{pv} - L_h/\eta_{inv} > 0$, the remainder is used to charge the BESS subject to the battery state of $SOC_{min} \leq SOC_i < SOC_{max}$. When the BESS gets fully charged according to SOC_{max}, the remainder is then dumped or sold to the grid. SOC_{max} is taken as battery capacity is this model.

Level 2

When P_{pv} is less than the load factored with inverter efficiency, $P_{pv} < L_h/\eta_{inv}$, the BESS discharges to the load subject to $SOC_{min} \leq SOC_i < SOC_{max}$ and $L_h/\eta_{inv} - P_{pv}$

Level 3

When the PV and the BESS cannot meet the load power requirements, the grid supplies electricity to the load in the given time, L_h. The grid is also used to charge the BESS for the condition $SOC_{min} \leq SOC_i < SOC_{max}$ until the battery state SOC_{max} is reached.

Level 4

When the both the PV and the BESS cannot meet the energy demand and in the absence of the grid due to load shedding, then the DG is ramped up to meet the demand load. The DG will also charge the BESS subject to DG - L_h/η_{inv} - P_{pv} and $SOC_{min} \leq SOC_i < SOC_{max}$

3.5.6 Modelling the Energy flow of the Grid connected PV – BESS – DG System

3.5.6.1 Modelling the PV array Output

The power from the PV would be calculated in each hour using equation

$$P_{pv} = \eta_{ref}\,[1 - 0.9\beta(T_{c,NOCT} - T_{a,NOCT})I_{pv}/I_{pv,NOCT} - \beta\,(T_a - T_{ref})]\,I_{pv} * A \quad (3.5.3)$$

$$\text{And } I_{pv} = K_{gr}\,I_o + (I_o - K_{gr}\,I_o)\,\frac{\cos\theta}{\cos\theta z} \text{ or } I_o(K_{gr} + (1 - K_{gr})\,\frac{\cos\theta}{\cos\theta z}) \quad (3.5.4)$$

η_{ref} = from the manufacturer, usually 15%, and the author used 15% in the model.

β = 0.0046

$T_{c,NOCT}$ = 45 ^oC

$T_{a,NOCT}$ = 20^oC

$I_{pv,NOCT}$ = 800 W/m^2 (2.88 MJ/m^2/h), at wind speed 1m/s

T_{ref} = 25 ^oC

3.5.6.2 Modelling the BESS Output

Then BESS will be modelled on 2 scenarios

When P_{pv} > Load, the battery will be charged, B_{ch}

B_{ch} = - MIN(η_{bat} ($\eta_{inv}P_{pv}$ - L_h), SOC_{max} - SOC_i) which can be solved in a Microsoft excel spreadsheet.

When P_{pv} < Load

The BESS discharges (B_{disch}) according to the logic below

B_{disch} = - MIN(L_h – $\eta_{inv}P_{pv}$, SOC_i – SOC_{min})

The BESS will also be charged by the grid or diesel generator for the condition SOC_i – SOC_{min}

In the model, it is proposed to use a battery sizing parameter, B_{cap}/L_{day}, that is the battery capacity as a fraction of the given daily Load.

Battery life is estimated using equation from the effective battery discharges given by equation 2.7.2.

3.5.7 Modelling the Diesel Generators Output

The DG is modelled according to the equations in Section 2.8

3.6 The Model Sizing and Optimisation

3.6.1 The Inputs

The main objective of the model is to reduce energy cost and CO_2 emission while achieving high reliability of energy supply. To measure the success of the study, the model will first establish the baseline, which is the Grid only, to supply the load and. The baseline will give the energy cost (as per the tariff rates) as well as the supply reliability which (reliability) is a function of the load shedding program. The study will model the next scenario before penetration of REs; being integrating DGs to provide back-up power in the absence of grid power. For this scenario, the energy cost, the supply reliability and the CO_2 emission will be calculated. The study will note that

DGs improve energy supply reliability from scenario 1 of grid only. Being a gold mine, it is more expensive to lack supply of energy.

The model results from scenario 1 and 2 will then be compared to simulation results of the HRES and the success of the study will be measured for significant reduction in energy cost, O and M costs of the DG and CO_2 reduction while improving supply reliability.

Supply reliability in this study is defined as the loss of load fraction (LLF) and will be calculated in two conditions; the 'strict' one as the fraction of hours when the energy supply system fails to completely satisfy the load and the 'partial' when the load satisfied is expressed as the fraction of the total load demand. LLF can be pre-set then different combinations of HES component sizes will be generated to achieve the LLF at the lowest optimized cost, Hove and Tazvinga (2012).

In the study, the initial battery state, SOC_i is taken as SOC_{max} where SOC_{max} is given by $DOD*B_{cap}$. The Grid will be selected and deselected including also the PV and the BESS.

3.6.2 The HES Model Sizing Curves

In the study, a dimensionless component for PV area is introduced, A / A_o. A is the actual PV area. The parameter A_o is defined by Hove (2000) as hypothetical area that would be required to meet the daily load demand if the irradiance is the nominal 1000W/m^2 and the PV efficiency is the reference value over all the 24 hours in a day. Mathematically stated;

$$A_o\ (m^2) = \frac{\mathrm{Lday\ (Wh)}}{\eta \mathrm{ref} * 24\mathrm{hr} * 1000\mathrm{W/m2}}$$

The battery in the BESS is sized according to B_{cap}/L_{day}

The DG is sized by the variable variable Q_{DG}/d where d is $L_{day}/24$ – the daily average load. The DG can also be sized according to the peak load, hence Q_{DG}/d_p.

The model will be governed by the three variables A/A_o, B_{cap}/L_{day} and Q_{DG}/d. In the model, two of the parameters will; be kept constant while varying the third one. For example, a DG and a certain B_{cap}/L_{day} will be kept constant whilst varying PV Array. Likewise, PV Array and a DG will be fixed while varying B_{cap}/L_{day}.

The model will also depend on other technical specifications and constraints:

- PV: Reference power output, reference efficiency, including inverter efficiency
- BESS: Battery efficiency (at charge and discharge, DOD, maximum battery charging power / current
- Load: Load per day, L_{day} including the loading shedding of the case study area.
- DG dispatch strategy $0.3Q_{DG} \leq d_{ON} \leq Q_{DG}$
- BESS Status $SOC_{min} \leq SOC_i < SOC_{max}$

An excel spreadsheet was developed for the energy flow control logic in table 3. From the spreadsheet, various values of LLF were calculated from the varying of the 3 variables A/A_o, B_{cap}/L_{day}, Q_{DG}/d, the DG dispatch strategy and the BESS constraint.

Model sizing curves were generated for the DG dispatch strategy for a target value of LLF. The size of the PV (A/A_o) was varied against the storage size, B_{cap}/L_{day}.

In the next stage of the optimization, the PV (A/A_o) was fixed and for a target value of LLF, the size of the DG, Q_{DG}/d, was varied against storage size B_{cap}/L_{day}.

Optimisation process was then repeated with BESS storage (B_{cap}/L_{day}) fixed whilst varying PV (A/A_o) and the DG size, Q_{DG}/d.

3.7 The HES Economic Cost Model

All model simulations are based on the life of the PV Array i.e. the project life. The life of the PV in this study is 25 years based on the performance warranty given by the manufacturer. The reader should be advised that the manufacturer specified a loss of performance of 2.5% in the first year and a subsequent linear degradation of 0.67% from year 2 to the rest of the PV life, i.e. 25th year. For this study, to simply the simulation, the calculations do not factor in degradation.

Costs associated with this study are split as:

- Capital costs – procurement and installation of HRES components; PV panels, BESS, charge controllers, inverters, cabling.
- O and M Costs – fuel cost, routine maintenance costs for DG, PV Array, BESS
- Replacement costs – costs cover replacement of HRES components whose life is shorter than the project life. DGs already installed, will be replaced.

3.7.1. Determination of the cost of energy

The cost of energy is determined through the following steps:

- Net Present Cost for each HRES Component is calculated for each year as the discounted costs up to the project life (lifespan of the PV) and summed up for the HRES components. The NPC formula is given below;

$$NPC = C_o + \sum_{n=1}^{n} \frac{OMC}{(1+r)^n} + \sum_{m=1}^{M} \frac{RC}{(1+r)^m} - \frac{(M+1)tR-n}{tR} \cdot \frac{RC}{(1+r)^n} \quad (3.7.1)$$

Where

C_o = capital cost of HRES component

n = project lifecycle, life of PV

OMC = Operation and Maintenance cost for an HRES component

r = Discount rate, interest rate

M = Number of times and HRES has to be replaced during the project's lifecycle

RC = Replacement cost of an HRES component

t_R = life of an HRES component

The last term from thr NPC equation is the net residual value of the replace3d HRES component.

For the PV, t_R is equal to 'n' and hence the residual value is zero. The NPC equation for PV reduces to;

$$NPC_{PV} = C_o + \sum_{n=1}^{n} \frac{OMC}{(1+r)^n} + \sum_{m=1}^{M} \frac{RC}{(1+r)^m} \quad (3.7.2)$$

For the DG, C_o is zero since they are already installed. The NPC equation for DG reduces to;

$$NPC_{DG} = \sum_{n=1}^{n} \frac{OMC}{(1+r)^n} + \sum_{m=1}^{M} \frac{RC}{(1+r)^m} - \frac{(M+1)tR-n}{tR} \cdot \frac{RC}{(1+r)^n} \quad (3.7.3)$$

Thus for the HES, the NPC becomes

$$NPC_{HRES} = NPV_{PV} + NPV_{BESS} + NPV_{DG} \quad (3.7.4)$$

For each HRES component other than the PV, M is calculated as the integer value of the quotient of $\frac{n}{tR}$ in the formula below;

$$M = INT\left(\frac{n}{tR}\right)$$

3.7.2. Annualised Cost (AC) of the HRES Model

AC of the HRES is found as a product of the NPC and the cost recovery factor (CRF)

$$AC = NPC_{HRES} \times CRF$$

$$CRF = \frac{r(1+r)^n}{(1+r)^n-1}$$

Cost of Energy for the HRES Model

The cost of energy (COE) is found by dividing the annual energy delivered to the load, E_a, into the HRES annualized cost (AC).

$$COE = \frac{AC}{Ea}$$

The COE is used in the model simulation to evaluate feasibility of HRES and as a measure to compare energy performance of each optimisation of the HRES described in the Model sizing section.

The model will be subject to economic factors to test its feasibility. These factors include the lifespan of the system components (Battery, PV Array), capital costs (PV, inverter, battery) and the operation and maintenance costs (PV, Inverter, Battery and the DG) including also the capacities of the HRES components. The capital cost of the DG is not included as DGs are already installed providing back-up power.

3.8 The Model Outputs

The model will give as its output, the hourly energy balance of the HRES, the PV Array power required, BESS capacity and inverter power rating. Output will also give the electricity consumption, Solar fraction, RE fraction, the energy supply reliability, the PV energy sold to the grid, operation and maintenance costs of the HRES, capital costs, energy costs per kWh and the CO_2 emission.

The capital costs for the system components were obtained from vendor websites, particularly vendors in China and India.

3.8.1 The Load Met

The load met L_{met} is defined as the amount of delivered load in one year and its units can be kW or kWh. It is also variably expressed as a percentage of the total load demand.

$$\% L_{met} = \frac{\text{Lmet}}{\text{Total Load Demand}} \times 100\%$$

The minimum met Load, % L_{met}, can be used in the model as a simulation constraint since it relates to HES reliability to supply electrical energy or Loss of Load Probability. Scenarios giving L_{met} less than the minimum will be discarded.

3.8.2. Sensitivity Analysis of the Model

The optimised model is based on the inputs which might actually change in the project life or error associated with measurements; the price of diesel, for example is volatile and will change. Therefore, a “What if” analysis is carried out to investigate the impact of the potential variations or errors have on the optimised model.

Chapter 4 Results and Discussions

4.1 Results

The author gives outputs from the model in this chapter starting with costs that were sourced from websites of equipment vendors.

4.1.1 Economic Costs

ECONOMIC PARAMETERS			
PV array lifespan		25	years
Battery lifespan		10.000	years
Inverter lifespan		10	years
DG lifespan		5	years
PV capital cost		0.5	$/W
Battery cost		0.15	$/Wh
Inverter cost		0.3	$/W
DG cost		0.3	$/W
DG maintenance		15%	of capital costs/annum
Specific fuel consumption		0.35	litre/kWh
Fuel cost		1.28	$/litre
PV array maintenance		3%	of capital costs/annum
Inverter maintenance		5%	of capital costs/annum
Discount rate		10%	of capital costs/annum
Battery maintenance cost		10%	of capital costs/annum
Electricity price	Peak	0.13	$/kWh
	Standard	0.07	$/kWh
	Off-peak	0.04	$/kWh
Calculated energy cost		0.07	$/kWh
Maximum Demand		5.54	$/kWh

Table 4.1.1, Economic Parameters

4.1.2 The Baseline Status

Energy from the grid without backup

DAILY LOAD DEMAND		4384	kWh
A/Ao		0.0	
Bcap/Lday		0.00	
PV ARRAY POWER		0	kW
BATTERY CAPACITY		0.0	kWh
INVERTER POWER		0	kW
FUEL GENERATOR POWER		0.0	kW
Annual Generator Runtime		0.0	hours
Fuel Consumption		0.0	Litres
Annual Grid Electricity Consumption		983153	kWh
Supply Reliability -Strict		62%	
Supply Reliability -partial		62%	
Renewable Energy penetration		0.0%	
Dumped PV Energy		0.00	%
Total Capital	0		$
Operating Costs	0		$
Levelised Cost of Energy		0.083	$/kWh
NPV (compared to DG +GRID)	2,582,753		$
Greenhouse Gas Emissions - CO_2		0.00	tons
Greenhouse Gas Emissions - SO_2		0.00	kg
Greenhouse Gas Emissions - N_2O		0.00	kg

Table 4.1.2., The Baseline status

4.1.3 Grid with diesel generator back up

Grid with Diesel Back up

Performance Characteristics

DAILY LOAD DEMAND		4384	kWh
A/Ao		0.0	
Bcap/Lday		0.00	
PV ARRAY POWER		0	kW
BATTERY CAPACITY		0.0	kWh
INVERTER POWER		0	kW
FUEL GENERATOR POWER		200.9	kW
Annual Generator Runtime		3344.0	hours
Fuel Consumption		207515.5	Litres
Annual Grid Electricity Consumption		983153	kWh
Supply Reliability -Strict		100%	
Supply Reliability -partial		100%	
Renewable Energy penetration		0.0%	
Dumped PV Energy		0.00	%
Total Capital	60,284		$
Operating Costs	274,662		$
Levelised Cost of Energy		0.234	$/kWh
NPV (compared to DG +GRID)	(0)		$
Greenhouse Gas Emissions - CO_2		599.70	tons
Greenhouse Gas Emissions - SO_2		24.28	kg
Greenhouse Gas Emissions - N_2O		4.86	kg

Table 4.1.3 Grid with diesel generator back up

4.1.4 System Design Curves

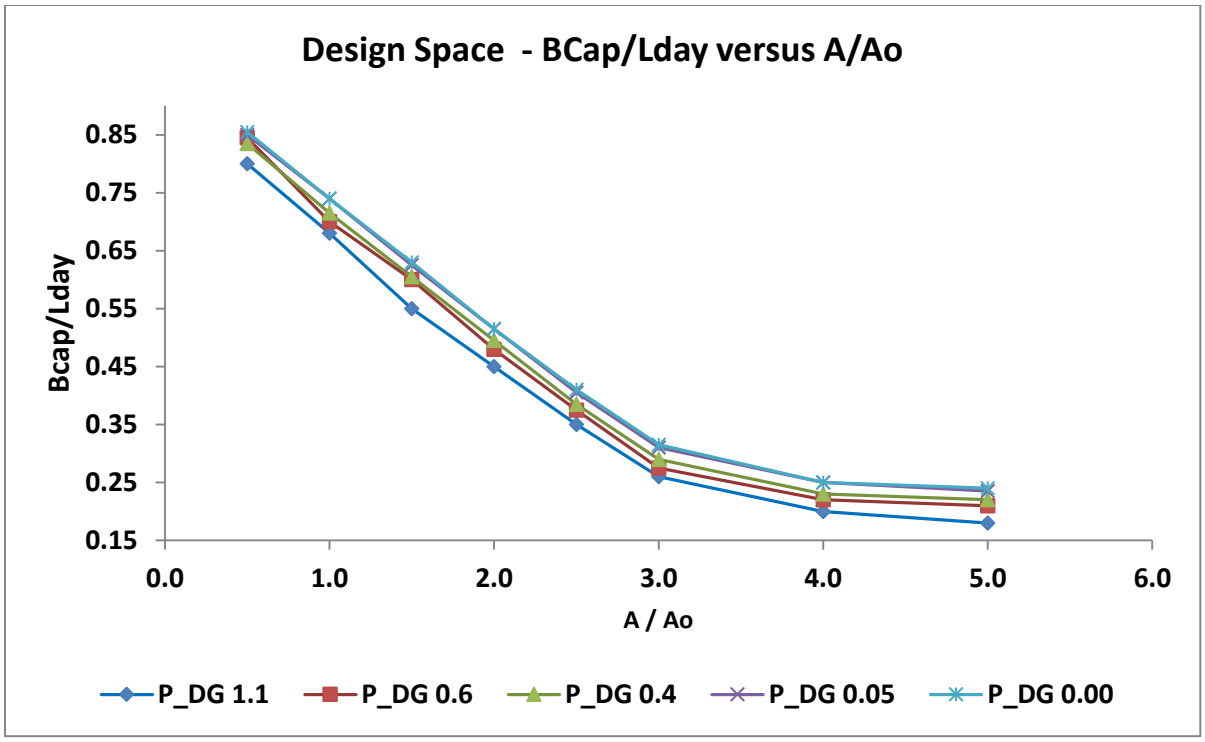

Fig 4.1 Design Space – Bcap/Lday

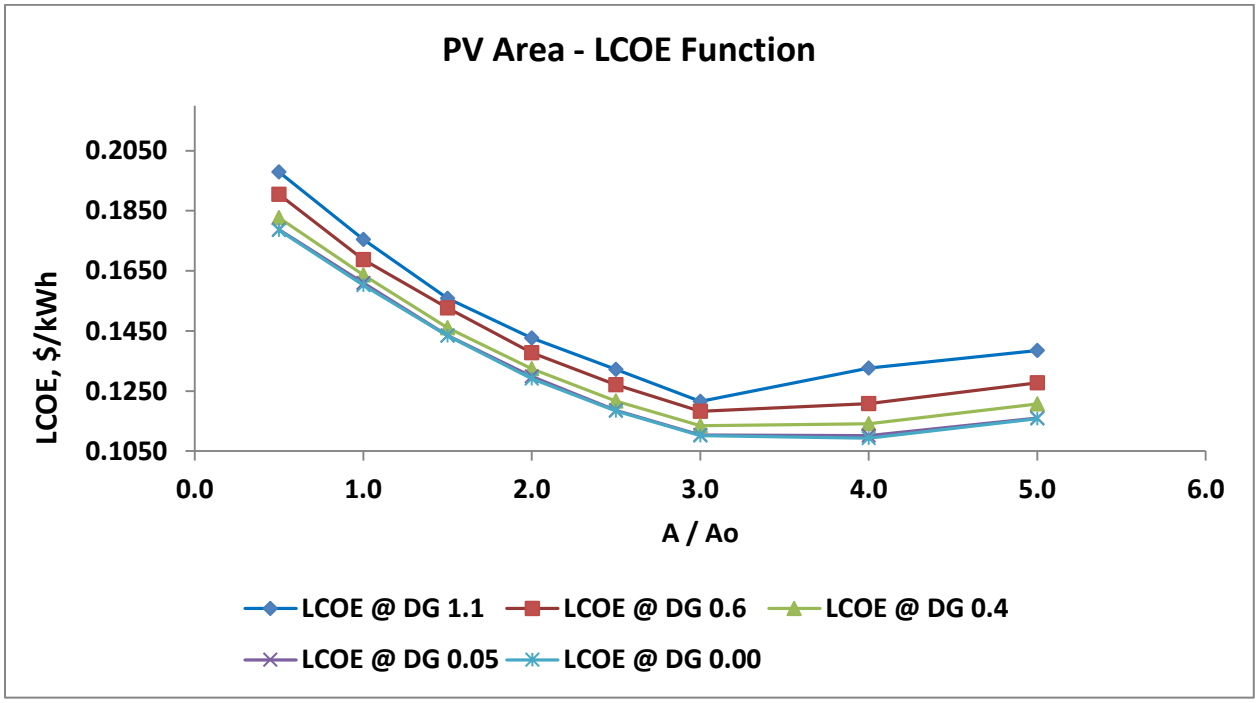

Fig 4.2 PV Area (A/Ao) – LCOE Function

4.1.5 System Specification

HES Model Sizing, Energy and Economic

PV-BESS-Grid-DG

DAILY LOAD DEMAND		4384	kWh
A/Ao		3.0	
Bcap/Lday		0.26	
PV ARRAY POWER		548	kW
BATTERY CAPACITY		1139.9	kWh
INVERTER POWER		237	kW
FUEL GENERATOR POWER		200.9	kW
Annual Generator Runtime		23.0	hours
Fuel Consumption		1405.2	Litres
Annual Grid Electricity Consumption		848518	kWh
Supply Reliability -Strict		100%	
Supply Reliability -partial		100%	
Renewable Energy penetration		60.7%	
Dumped PV Energy		6.86	%
Total Capital	576,408		$
Operating Costs	39,717		$
Levelised Cost of Energy		0.122	$/kWh
NPV (compared to DG +GRID)	1,544,900		$
Greenhouse Gas Emissions - CO_2		4.06	tons
Greenhouse Gas Emissions - SO_2		0.16	kg
Greenhouse Gas Emissions - N_2O		0.03	kg

Table 4.1.5 HES Model Specification

4.1.6 Load Sharing Profiles by the HES Model

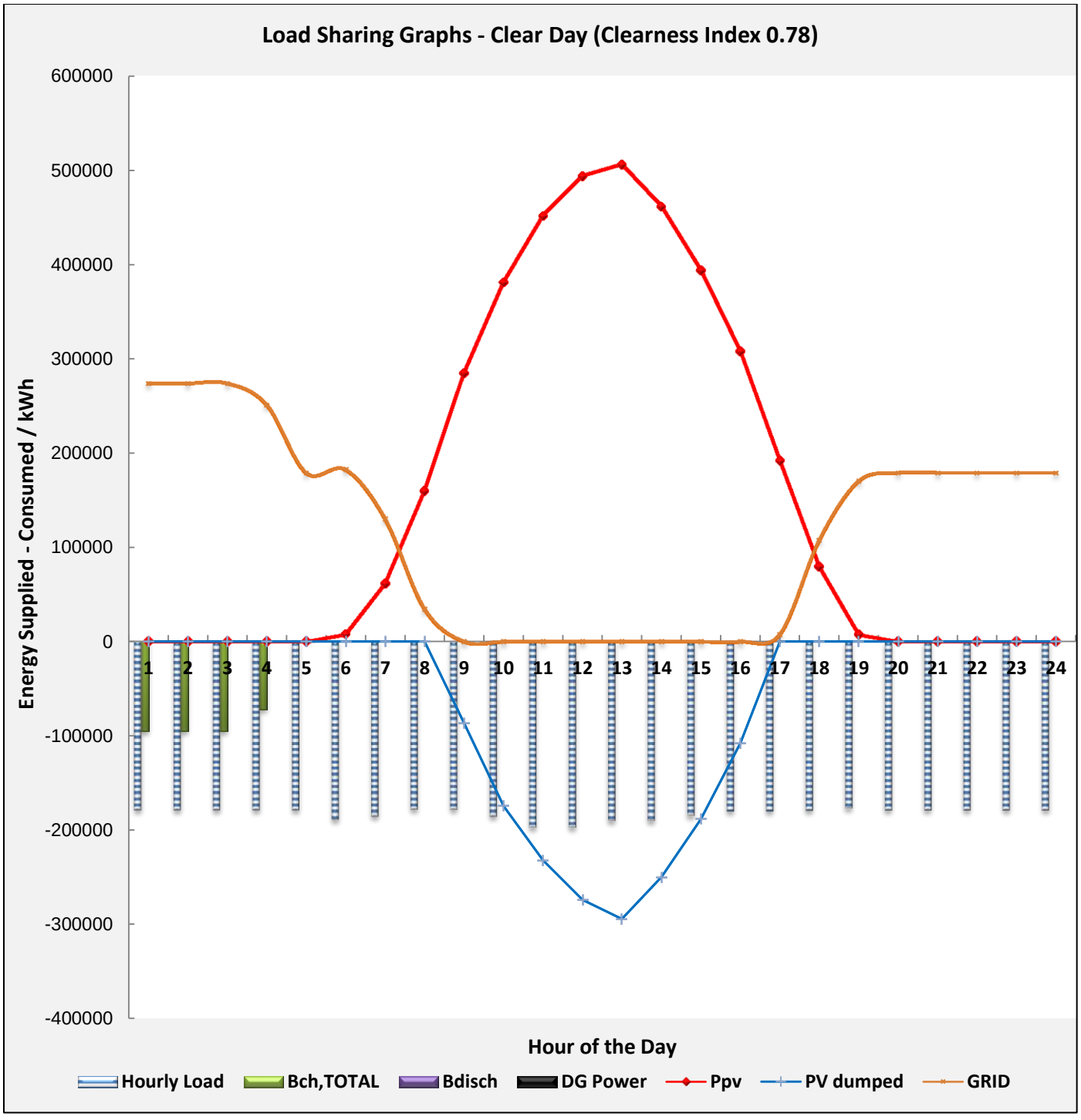

Fig 4.3 Load Sharing on a clear day

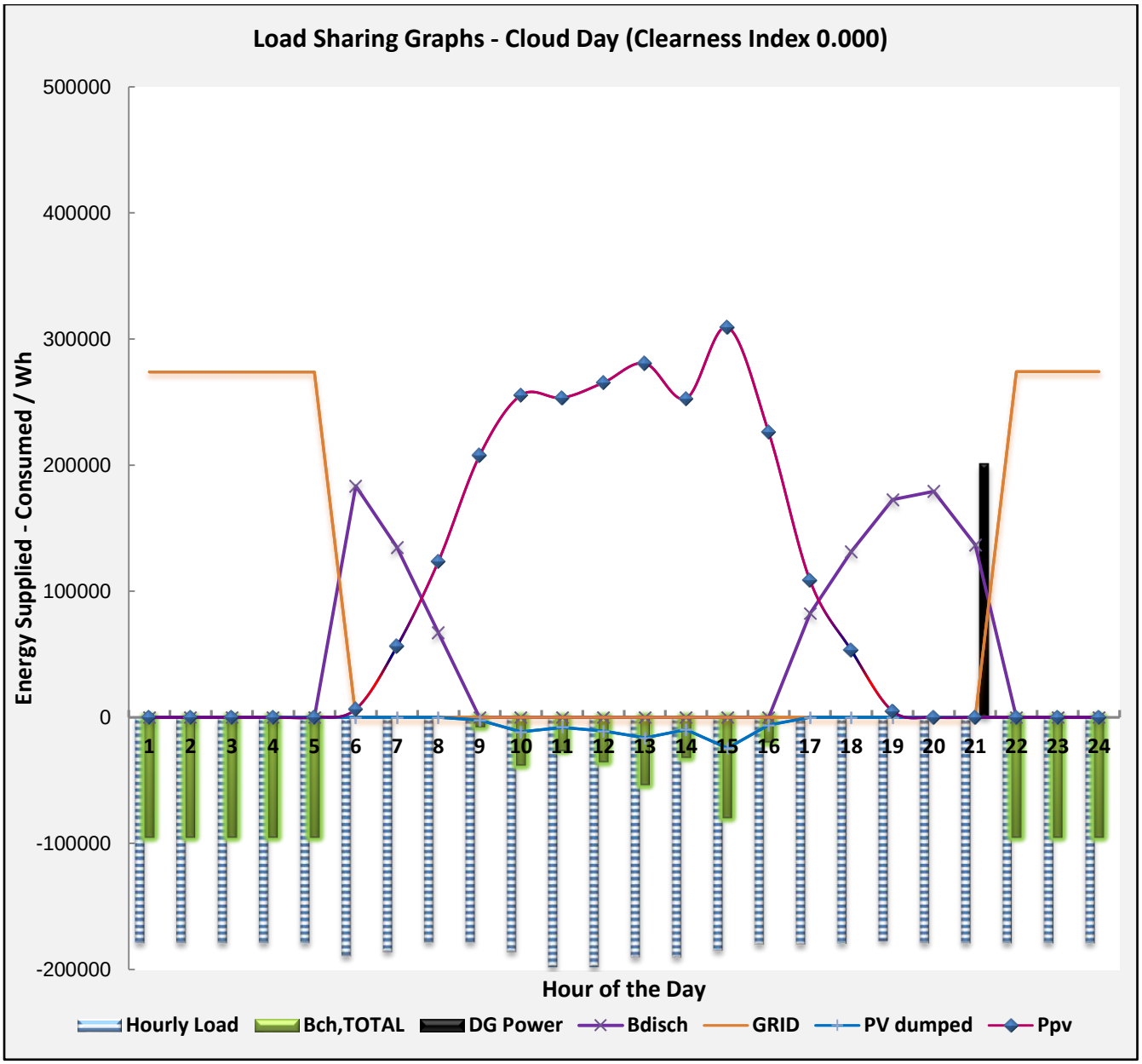

Fig 4.4 Load Sharing on a cloudy day

4.1.7 Sensitivity Analysis on the Model

Table 4.5 Sensitivity Analysis on the HES Model for Variation in fuel, PV capital costs and electricity tariffs

GridPVBESSDG			Fuel Costs			PV Cost			Electricity Tariff			
			1.4	1.3	1.2	0.45	0.4	0.3	1.05	1.1	1.15	1.2
DAILY LOAD DEMAND	kWh	**4384**	4384	4384	4384	4384	4384	4384	4384	4384	4384	4384
A/Ao		**3.00**	3.00	3.00	3.00	3.00	3.00	3.00	3.00	3.00	3.00	3.00
Bcap/Lday		**0.26**	0.26	0.26	0.26	0.26	0.26	0.26	0.26	0.26	0.26	0.26
PV ARRAY POWER	kW	**548**	548	548	548	548	548	548	548	548	548	548
BATTERY CAPACITY	kWh	**1140**	1140	1140	1140	1140	1140	1140	1140	1140	1140	1140
INVERTER POWER	kW	**237**	237	237	237	237	237	237	237	237	237	237
FUEL GENERATOR POWER	kW	**201**	201	201	201	201	201	201	201	201	201	201
Annual Generator Runtime	hours	**23**	23	23	23	23	23	23	23	23	23	23
Fuel Consumption	Litres	**1405**	1405	1405	1405	1405	1405	1405	1405	1405	1405	1405
Annual Grid Electricity Consumption	kWh	**848518**	848518	848518	848518	848518	848518	848518	848518	848518	848518	848518
Supply Reliability - Strict	%	**100%**	100%	100%	100%	100%	100%	100%	100%	100%	100%	100%
Supply Reliability - partial	%	**100%**	100%	100%	100%	100%	100%	100%	100%	100%	100%	100%
Renewable Energy penetration	%	**60.7%**	60.7%	60.7%	60.7%	60.7%	60.7%	60.7%	60.7%	60.7%	60.7%	60.7%
Dumped PV Energy	%	**686%**	7	7	7	7	7	7	7	7	7	7
Total Capital	$	**576,408**	576,408	576,408	576,408	549,006	521,604	466,800	576,408	576,408	576,408	576,408
Operating Costs	$	**39,717**	39,885	39,745	39,604	38,894	38,072	36,428	39,717	39,717	39,717	39,717
Levelised Cost of Energy	$/kWh	**0.12152**	0.12163	0.12154	0.12145	0.11903	0.11653	0.11155	0.12301	0.12450	0.12599	0.12748
NPV (compared to DG +GRID)	$	**1,544,900**	1,769,405	1,582,318	1,395,231	1,580,586	1,616,272	1,687,644	1,548,285	1,551,670	1,555,054	1,558,439
Greenhouse Gas Emissions - CO_2	tons	**4.06**	4	4	4	4	4	4	4	4	4	4
Greenhouse Gas Emissions - SO_2	kg	**0**	0	0	0	0	0	0	0	0	0	0

Greenhouse Gas Emissions - N_2O	**kg**	**0**	0	0	0	0	0	0	0	0	0	0

4.1.8 HES Model Architecture

4.1.8.1 HES Model Architecture by numerical simulation method

HES System Components

PV Array

- 3654 m^2 actual PV area
- Sun Fuel Technologies India - SFTI - 300 Modules
- Array Voltage 1000V
- Modules per string 24
- Number of parallel Strings 83
- Total number of modules 1980

Inverter

- 206kW Rating
- $V_{in} = V_{out}$ = 1000 DC
- I = 181

Battery System

- 83 x 12V

4.1.8.2 HES Model Architecture by Intuitive simulation method

HES System Components

PV Array

- 5617 m^2 actual PV area
- Sun Fuel Technologies India - SFTI - 300 Modules
- Array Voltage 1000V
- Modules per string 21
- Number of parallel Strings 145
- Total number of modules 3045

Inverter

- 206kW Rating
- $V_{in} = V_{out} = 1000$ DC
- I = 183
- Inverter Efficiency at 90%

Battery System

- Lead Acid Battery
- 83 x 12V
- Charge controller efficiency at 85%

4.2 Discussions

4.2.1 Model Development and the baseline

The general model was developed and was applied to the case study in which the LCOE was estimated at 8c/kWh based on time of use and maximum demand estimations. The reliability is however much lower at 62% at this scenario and is estimated from load shedding program.

4.2.2 Model Application to Grid and DG scenario

In order to increase energy supply reliability in the operation, the operations are powered by the DG. The model estimated that the even though the reliability increased to 100%, the LCOE increased 187.5% to 23/kWh due to fuel costs and operation and maintenance costs of the DG. Further, model estimates that 600 tonnes of CO2 are emitted by the DG operation and this scenario negates the global thrust to reduce consumption of finite and fossil fuels – fossil fuels being significant contributors to the GHG emissions

4.2.3 System Design curves

For a set P-DG, the required B_{cap}/L_{day} reduces with increase in A/A_o. However, at reaching A/A_o = 3, the rate of reduction in required B_{cap} reduces. Beyond, A/A_o = 3 the system design begins to flatten as depicted in the figures in Chapter 4. Also, the LCOE which reached a minimum at 3.0, begins to rise. Hence, the system components are derived from the LCOE minimum – A/A_o = 3, B_{cap}/L_{day} is 0.26.

The P-DG can be further reduced. In the model, this shifted the B_{cap}/L_{day} versus A/A_o curve upwards whilst the LCOE versus A/A_o shifted downwards. This implies with reduced P-DG, the required battery storage increases. Further, the LCOE reduces. In this model, the author reduced the P-DG from 1.1 to 0.0. In all cases the LCOE reduced and no curving upwards of the LCOE was observed to establish a minimum B_{cap}/L_{day}. This could be due to the economic costs used which reflect ever falling prices in the PV, batteries and Inverters compared to the high cost of diesel fuel.

4.2.4 Model Application for HES Model (PV-BESS-Grid-DG)

The model simulated the above HES configuration and yielded an optimum system combination giving a power supply reliability of 100%, reduced LCOE of 12c/kWh, reduced GHG emission of 4 tonnes of CO2 per annum and a significant renewable energy penetration of 62%. Further, the HES gives a positive NPV of $1,544,900 compared with the current Grid and DG scenario. The HES model is based on A/Ao of 3, B_{cap}/L_{day} of 0.26 and P-DG of 1.1.

From the analysis given in section 5.3, a scenario was be established when DG would be eliminated from the HES model while B_{cap}/L_{day} increased to 0.85 and the LCOE was estimated at 11c. However, to be able to meet energy supply reliability of 100% in the event of continuous period of cloud cover and in absence of grid after storms, hence PV and BESS will not be adequate to meet load requirements, the author decided to set the P-DG at 1.1. The author could not therefore justify the elimination of the DG to save 1c/kWh at increased risks of failing to meet power demand.

4.2.5 Load Sharing Profiles for HES Model (PV-BESS-Grid-DG)

The model gives load sharing profiles for a typical clear day when no DG would be used and a cloudy day with no grid. The profiles depict a diurnal day from midnight to midnight.

4.2.5.1 Clear day

The load sharing profile was done for a clear day. The model depicts time starting at midnight when grid is present and PV is absent. The grid powers the load and charges the battery until Bcap is reached at 4am from which time the demand on the grid is reduced. From 6am to 9am, PV generated is recorded and increases during which time interval the demand on the grid further falls until 9am when it is falls to zero due to adequate PV generated power. PV power generated peaks at 12pm midday and falls until 5pm.

In the time interval 9am to 5pm, excess PV power beyond the load demand is dumped. Due to high PV power on a clear day and to a healthy battery state, and hence no battery charging, the dumped PV power is significant – the total dumped energy for the clear day is 1659kWh. From 5pm when PV power further reduces until zero at 7pm, power is drawn from the grid to make up for the PV deficiency. From 7pm, when PV is zero, the grid takes over the load until midnight.

4.2.5.2 Cloud day

The load sharing profile was done for a cloud day. The model depicts time starting at midnight when grid is present and PV is absent. The grid powers the load and charges the battery until Bcap is reached at 5am from which time the demand on the grid is off due to load shedding. The battery discharges to meet the load demand. From 6am to 9am, PV generated is recorded and increases during which time interval the demand on the discharge from battery falls until 9am when it is falls to zero due to adequate PV generated power. PV power generated peaks at 12pm midday and falls until 5pm.

In the time interval 9am to 5pm, excess PV power beyond the load demand is dumped as there is no charging due to a healthy battery state. Also, due to lower PV power on a cloud day compared to a clear day, the dumped PV power is less significant – the total dumped energy for the cloud day is only 124kWh. From 5pm when PV power further reduces until zero at 7pm, battery discharges to make up for the PV deficiency. From 7pm, when PV is zero, the battery discharges for a further 2 hours. At 9pm, the DG ramps up to provide power to the load due to state of charge approaching set minimum SOC. Grid power returns at 10pm and from that time, powers the load and charges the battery until midnight.

4.2.6 Sensitivity Analysis on the HES Model (PV-BESS-Grid-DG)

PV capital costs, fuel price and electrical tariffs were varied to accommodate the errors that might have generated at defining economic costs.

4.2.6.1 Fuel Costs Increase

In all situations, increase in fuel price from $1.28 to $1.4/L, increased the NPV of the HES as compared to the Grid and DG scenario from $1,544,900 to $1,769,144. As the diesel consumption is significant in the Grid and DG scenario with a DG runtime of 3344 hours, fuel consumption is significant at about 207,516 L. An increase favours the introduction of PV and BESS into the energy mix. A reduction in the fuel price to $1.20/L on the other hand reduces the NPV of the HES model compared to that of Grid and DG to $1,395,231 but it remains positive and significant still making the HES model an economic solution.

4.2.6.2 PV Capital Costs decrease

The cost were set at $0.5/W. The author notes that the costs are trending lower (costs at $0.3/W were reported) and with reduced PV costs, the NPV of the HES model further increases to an NPV of $1,687,644, making the HES model a viable solution – thus supporting the introduction of PV and BESS into the energy mix.

4.2.6.3 Electrical Costs Increase

Due to widely reported electrical power shortages, and hence increasing power imports, the author bases the analysis on increasing tariffs. In the HES model less grid energy is consumed (848,518kWh), compared to the Grid and DG scenario (983153 kWh). Increase in electrical tariffs from 5 to 20%, result in an increase of NPV from $1,544,900 through to $1,558,439.

The author also wants to state that the slight increase of $13,539 in the NPV value even when the HES model consumes significantly lower electrical power of 134,635kWh, the average tariff price already low at 8c/kWh just increased to 9.6c/kWh.

Therefore, the diesel fuel and the PV cost have significant impact on the viability of the HES model compared to the electrical tariff. In the analysis above, the HES remains an economic and feasible solution to address the low reliability of the mine.

Chapter 5 Economic Analysis

5.1 Economic Parameters

The HES model was developed with the following economic parameters;

ECONOMIC PARAMETERS			
PV array lifespan		25	years
Battery lifespan		10.000	years
Inverter lifespan		10	years
DG lifespan		5	years
PV capital cost		0.5	$/W
Battery cost		0.15	$/Wh
Inverter cost		0.3	$/W
DG cost		0.3	$/W
DG maintenance		15%	of capital costs/annum
Specific fuel consumption		0.35	litre/kWh
Fuel cost		1.28	$/litre
PV array maintenance		3%	of capital costs/annum
Inverter maintenance		5%	of capital costs/annum
Discount rate		10%	of capital costs/annum
Battery maintenance cost		10%	of capital costs/annum
Electricity price	Peak	0.13	$/kWh
	Standard	0.07	$/kWh
	Off-peak	0.04	$/kWh
Calculated energy cost		0.07	$/kWh
Maximum Demand		5.54	$/kWh

Table 5.1

5.2 HES Model Cost - Annual

The economic costs for HES model are summarized in the table below

	$		
DG capital cost	60284.38	System voltage	12
PV capital cost	274019.91	Cycle life, Lr	1200
Inverter capital cost	71115.30	Rated depth of dischargeDODr	0.5
Battery capital cost	170988.42	Rate capacity 'amp-hours', C_R	94994
DG maintenance cost	9042.66	Life thru'put	#########
PV maintenance cost	8220.60		
Inverter maintenance cost	3555.77	sum_Deff	6913185.57
Battery maintenance cost	17098.84	Batt life	10.00
Total capital cost	576408.01	round 3	10.00
Annual maintenance costs	37917.86	round 2	10.00
		round 1	10.00

Table 5.2 HES Model Cost

5.3 HES Model Cost – Project Lifetime Costs

HRES Project Costs									
Year	CAPITAL +MAINTENANCE+REPLACEMENT	FUEL	GRID ENERG	PV exporte	Net import	TOTAL	DF	PV	Cum PV
0	614325.87	0	0	0	0	614325.87	1.0000	614325.87	614325.87
1	37917.86	1798.64	60137.57	45261.96	14875.60	99854.07	0.9091	90776.43	705102.29
2	37917.86	1798.64	60137.57	44809.34	15328.22	99854.07	0.8264	82524.02	787626.32
3	37917.86	1798.64	60137.57	44361.25	15776.32	99854.07	0.7513	75021.84	862648.16
4	37917.86	1798.64	60137.57	43917.64	16219.93	99854.07	0.6830	68201.67	930849.83
5	98202.24	1798.64	60137.57	43478.46	16659.11	160138.45	0.6209	99433.38	1030283.21
6	37917.86	1798.64	60137.57	43043.68	17093.89	99854.07	0.5645	56365.02	1086648.23
7	37917.86	1798.64	60137.57	42613.24	17524.33	99854.07	0.5132	51240.93	1137889.15
8	37917.86	1798.64	60137.57	42187.11	17950.46	99854.07	0.4665	46582.66	1184471.81
9	37917.86	1798.64	60137.57	41765.24	18372.33	99854.07	0.4241	42347.87	1226819.68
10	340305.96	1798.64	60137.57	41347.58	18789.98	402242.17	0.3855	155081.77	1381901.45
11	37917.86	1798.64	60137.57	40934.11	19203.46	99854.07	0.3505	34998.24	1416899.69
12	37917.86	1798.64	60137.57	40524.77	19612.80	99854.07	0.3186	31816.58	1448716.28
13	37917.86	1798.64	60137.57	40119.52	20018.05	99854.07	0.2897	28924.17	1477640.45
14	37917.86	1798.64	60137.57	39718.32	20419.24	99854.07	0.2633	26294.70	1503935.14
15	98202.24	1798.64	60137.57	39321.14	20816.43	160138.45	0.2394	38335.87	1542271.01
16	37917.86	1798.64	60137.57	38927.93	21209.64	99854.07	0.2176	21731.15	1564002.17
17	37917.86	1798.64	60137.57	38538.65	21598.92	99854.07	0.1978	19755.60	1583757.76
18	37917.86	1798.64	60137.57	38153.26	21984.30	99854.07	0.1799	17959.63	1601717.40
19	37917.86	1798.64	60137.57	37771.73	22365.84	99854.07	0.1635	16326.94	1618044.33
20	340305.96	1798.64	60137.57	37394.01	22743.55	402242.17	0.1486	59790.74	1677835.07
21	37917.86	1798.64	60137.57	37020.07	23117.49	99854.07	0.1351	13493.34	1691328.41
22	37917.86	1798.64	60137.57	36649.87	23487.69	99854.07	0.1228	12266.67	1703595.08
23	37917.86	1798.64	60137.57	36283.37	23854.19	99854.07	0.1117	11151.52	1714746.59
24	37917.86	1798.64	60137.57	35920.54	24217.03	99854.07	0.1015	10137.74	1724884.34
25	98202.24	1798.64	60137.57	35561.33	24576.23	160138.45	0.0923	14780.14	**1739664.48**

Table 5.3 HES Model Cost

5.4 HES Model NPV compared to Grid and Diesel Scenario

	NPV Analysis against GRID - DG System as Baseline					
Year	Total Cost, A Proposed	Cost, B GridDG	B - A	DF	PV Costs	Cum PV
0	614325.87	69327.04	-544998.83	1.000	-544998.83	-544998.83
1	99854.07	344342.13	244488.06	0.909	222261.87	-322736.96
2	99854.07	344342.13	244488.06	0.826	202056.25	-120680.71
3	99854.07	344342.13	244488.06	0.751	183687.50	63006.79
4	99854.07	344342.13	244488.06	0.683	166988.63	229995.42
5	160138.45	404626.51	244488.06	0.621	151807.85	381803.27
6	99854.07	344342.13	244488.06	0.564	138007.14	519810.40
7	99854.07	344342.13	244488.06	0.513	125461.03	645271.44
8	99854.07	344342.13	244488.06	0.467	114055.48	759326.92
9	99854.07	344342.13	244488.06	0.424	103686.80	863013.73
10	402242.17	404626.51	2384.34	0.386	919.27	863932.99
11	99854.07	344342.13	244488.06	0.350	85691.57	949624.56
12	99854.07	344342.13	244488.06	0.319	77901.43	1027525.99
13	99854.07	344342.13	244488.06	0.290	70819.48	1098345.48
14	99854.07	344342.13	244488.06	0.263	64381.35	1162726.82
15	160138.45	404626.51	244488.06	0.239	58528.50	1221255.32
16	99854.07	344342.13	244488.06	0.218	53207.73	1274463.05
17	99854.07	344342.13	244488.06	0.198	48370.66	1322833.71
18	99854.07	344342.13	244488.06	0.180	43973.33	1366807.03
19	99854.07	344342.13	244488.06	0.164	39975.75	1406782.78
20	402242.17	404626.51	2384.34	0.149	354.42	1407137.20
21	99854.07	344342.13	244488.06	0.135	33037.81	1440175.01
22	99854.07	344342.13	244488.06	0.123	30034.37	1470209.39
23	99854.07	344342.13	244488.06	0.112	27303.98	1497513.36
24	99854.07	344342.13	244488.06	0.102	24821.80	1522335.16
25	160138.45	404626.51	244488.06	0.092	22565.27	1544900.43

Table 5.4 HES Model NPV compared to Grid and Diesel Scenario

Chapter 6 Recommendations

The author that further study to assess the impact of HES model on peak load shaving and hence LCOE has to be carried out. Peak load shaving will manage the maximum demand. The proposed study would quantify the benefits of the HES model.

From a general point of view PV tilt optimization is likely to reduce consumption of the diesel power. Thus, further work is required to quantify benefits of PV tilt optimization in the model especially on LCOE.

The author proposes long term radiation measurements to be made on site to verify satellite collected data.

In this study, the load profile was assumed the same for every day of the year. However this might not be case and thus model based on a constant load might be oversized or undersized. The author therefore recommends that the load profile be determined for a week and replicated for the year. The accuracy of the model might be improved.

Chapter 6 Conclusion

A general HES model with low LCOE, while meeting the 100% reliability constraint, was developed for small to medium industrial operations applications. The model was applied to a case study with a daily energy demand of 4.38 MWh and a peak load of 197kW.

General HES design curves were developed based on the load profile leading to the selection of the optimum HES for the case study.

For the case study in particular, the model achieved to meet the reliability constraint of 100%. The HES model was sized at A/ A_o of 3.0, B_{cap}/ L_{day} of 0.26 and DG at 1.1 of Load to achieve a LCOE of 12c/kWh against 23c/kWh of the grid and DG only. The model simulated a renewable energy penetration of 60% thereby reducing direct GHG annual CO_2 emissions to 4.0 tons from 600 tons with Grid and DG only.

The model achieved the objectives of a 100% supply reliability, low LCOE of 12c/kWh whilst increasing the uptake of renewables into the energy mix. Sensitivity anakyses use variation in fuel price, PV capital costs and electrical tariffs and the results showed the model offered an economic solution to achieve the 100% reliability constraint instead of using DG for back-up power.

The model can therefore be applied for sizing of other similar operations to institutions.

8. References

1. A.E.S.A. Nafeh, “Proposed Technique for Optimally Sizing a PV/Diesel Hybrid System”, Lu Zhang et al., Vol.2, No.4, 2012 696 International Conference on Renewable Energies and Power Quality, Spain, 23-25 March 2010, INTERNATIONAL JOURNAL of RENEWABLE ENERGY RESEARCH

2. Africa Progress Panel, 2015

3. Babu C.A., and S. Ashok (2009), “Optimal utilization of renewable energy-based IPPs for industrial load management,” Renewable Energy, vol. 34, pp. 2455-2460, Feb. 2009.

4. Bloomberg New Energy Finance, Q1 2017 OFF-GRID AND MINI-GRID MARKET OUTLOOK, 18 JANUARY 2017). Selected community mini-grids announced in 2016,

5. Bloomberg New Energy Finance, Q1 2017 OFF-GRID AND MINI-GRID MARKET OUTLOOK, 18 JANUARY 2017). Selected commercial and industrial applications announced in 2016,

6. Bortolini, M. Gamberi, M., and A. Graziani, “Technical and economic design of photovoltaic and battery energy storage system,” Energy Conversion and Management, vol. 86, pp. 81–92, 2014

7. Chedid

8. Chow, T.T. Performance analysis of PVT collector by explicit dynamic model. Solar Energy 2003; 75,143-152.

9. Daud Muhamad Zalani, Azah Mohamed, M.Z.C. Wanik, M. A. Hannan (2012), “Performance evaluation of grid-connected photovoltaic system with battery energy storage”, 2012 IEEE International Conference on Power and Energy (PECon), 2-5 December 2012, Kota Kinabalu Sabah, Malaysia

10. Denholma, P., and Margolis, R. M.,2007, “Evaluating the limits of solar photovoltaics (PV) in electric power systems utilizing energy storage and other enabling technologies,” Energy Policy, vol. 35, pp. 4424–4433, 2007.

11. Dihrab, S. S., and Sopian. K, 2010. Electricity generation of hybrid PV/wind systems in Iraq. Renew. Energy 35:1303–1307.

12. Duffie and Beckman (2013), Solar Engineering of Thermal Processes, 4th Edition, Wiley

13. Dufo-Lopez, R., and J. L. Bernal-Agustın. 2008. Multi-objective design of PV–wind–diesel–hydrogen–battery systems. Renew. Energy 33:2559–2572.

14. Drouilhet S.,1997, National Renewable Energy Laboratory B.L. Johnson Integrated Power Corporation "A Battery Life Prediction Method for Hybrid Power Applications" http://www.nrel.gov/docs/legosti/fy97/21978.pdf

15. Dursun, B., Gokcol, C., Umut,I., Ucar E., and Kocabey, S, 2013. Techno-economic evaluation of a hybrid PV—Wind power generation system. Int. J. Green Energy 10:117–136

16. Evans D.L., 1981 Simplified method for predicting photovoltaic array output. Solar Energy: 27-555.

17. Farmer, B.K., PVUSA Model Technical Specification for a Turnkey Photovoltaic Power System. Appendix C, p. c2, 1992

18. Furushima, K., Nawata, Y., Sadatomi, M.,. Prediction of photovoltaic power output considering weather effects. In: ASES Conference SOLAR 2006 – Renewable Energy Key to Climate Recovery. July 7–13, Denver, Colorado, 2006.

19. Hossain Asad, Md. Faisal Kabir, Rashad Kabir, Md. Rafiqul IslamOptimal On-Grid Hybrid Renewable Energy Model for Coastal Area : Bangladesh Perspective, 2nd International Conference on Green Energy and Technology, September 2014

20. Hottel, H. C. and B. B. Woertz, Trans. ASME, 64, 91 (1942). ''Performance of Flat-Plate Solar Heat Collectors.''

21. Hove, T., (2000) A method for predicting long-term average performance of photovoltaic systems, Renewable Energy, 21 (4), pp 207 - 229

22. Hove, T. and Mushiri, T, 2015, “Dimensioning of hybrid solar-battery-grid micro-energy power systems to alleviate domestic power outages in urban Zimbabwe: A reliability cost Approach”, Proceedings of the International Renewable Energy Symposium, Windhoek, Namibia

23. Hove, T. and Tazvinga, H, 2012, “A Techno-economic model for optimizing component sizing and energy dispatch strategy for PV-diesel-battery hybrid power systems, Journal of Energy in Southern Africa, **23**, 18 – 28 (2012)

24. http://homerenergy.com/pdf/ABB-Microgrids-Brochure.pdf, - ABB Microgrid Solutions: Advancing Sustainable and Reliable Energy Solutions).

25. http://www.camelottech.com/CMFiles/Docs/PT-7007-SizingGensets.pdf

26. http://www.raad-eng.com/techdata/cummins/QSK60G3.pdf

27. http://www.world-nuclear.org/information-library/facts-and-figures/heat-values-of-various-fuels.aspx - accessed 02 June 2017

28. International Energy Agency, 2015, World Energy Outlook 2015

29. International Energy Agency, 2016 - World Energy Outlook 2016

30. IPCC – Intergovernmental Panel on Climate Change 2006 - Guidelines for National Greenhouse Gas Inventories Volume 2., CHAPTER 2 STATIONARY COMBUSTION

31. Jacobus, H., et al. 2011. Evaluating the impact of adding energy storage on the performance of a hybrid power system. Energy Convers. Manage. 52:2604–2610.

32. Jeffy Marin Jose and Cherian, V. I., “ A review on design and cost analysis on hybrid power solution for remote telecom towers”, INTERNATIONAL JOURNAL OF CURRENT ENGINEERING AND SCIENTIFIC RESEARCH (IJCESR), 2015 VOLUME-2, ISSUE-7, 211 - 217

33. Kaldellis, J.K., 2007, “An integrated model for performance simulation of hybrid wind-diesel systems”, Renewable Energy, vol. 32, pp. 1544-1564, September 2007

34. Kalogirou, Solar thermal collectors and applications, 2004, Progress in Energy and Combustion Science, Volume 30, Issue 3, 2004, Pages 231–295, Elsevier

35. Kellogg, W.D., Nehrir, M.H., Venkataramanan, G., and Gerez, V., “Generation unit sizing and cost analysis for stand-alone wind photovoltaic and hybrid wind/PV systems”, IEEE Trans Energy Convers. 1998;13(1):70–75.

36. Khatib et al (2013), “Renewable and Sustainable Energy Reviews” 2013(22): 454–465

37. Kusakana, K., and H. J. Vermaak. 2013. Hybrid renewable power systems for mobile telephony base stations in developing countries. Renewable Energy 51:419–425.

38. Liu, B. Y. H. and R. C. Jordan, Solar Energy, 7, 53 (1963). ‘‘The Long-Term Average Performance of Flat-Plate Solar Energy Collectors.’’

39. Luque. A and Hegedus. S., “Handbook of Photovoltaic Science and Engineering”. John Wiley & Sons Ltd, The Atrium, Southern Gate, Chichester, West Sussex PO19 8SQ, England, pp. 296-297, 2003.

40. Marra F., and G. Yang, “Chapter 10 - decentralized energy storage in residential feeders with photovoltaics,” Energy Storage for Smart Grids, vol. 2015, pp. 277–294, 2015.

41. Meyer, E.L., van Dyk, E.E.. Development of energy model based on total daily irradiation and maximum ambient temperature. Renewable Energy 21, 37–47, 2000

42. Muguti V, Design of a Hybrid Solar Domestic Electrical Water Heating System, Mechanical Engineering, University of Zimbabwe, 2009, 53-54

43. Myles, Paul, Joe Miller, Steven Knudsen, and Tom Grabowski. 430.01.03 Electric Power System Asset Optimization. Morgantown, WV: National Energy Technology Laboratory, 2011.

44. Nandi, S. K., and H. R. Ghosh. 2010. Prospect of wind–PV-battery hybrid power system as an alternative to grid extension in Bangladesh. Energy 35:3040–3047.

45. Nandi, S. K., and Ghosh, H. R., 2010. Techno-economical analysis of off-grid hybrid systems at Kutubdia Island, Bangladesh. Energy Policy 38:976–980

46. Nottrott, A., Jan Kleissl, Byron Washom (2013), “Energy dispatch schedule optimization and cost benefit analysis for grid-connected, photovoltaic-battery storage systems”, Article in Renewable Energy 55:230-240·July2013

47. Nurunnabi, M., Roy NK., “Grid connected hybrid power system design using HOMER”, In Proceedings of the 2015 international conference on advances in electrical engineering (ICAEE) . IEEE; December 2015. p. 18–21

48. Olatomiwa, L. J. , S. Mekhilef, A.S.N. Huda, 2014, “Optimal Sizing of Hybrid Energy System ffor a Remote Telecom Tower: A Case Study in Nigeria,” IEEE Conference on Energy Conversion (CENCON), 3(1), pp.243-247, 2014.

49. Raja, I. A., Doggar, M.G., and Abro, R.S., “Solar energy application in Pakistan”, Conference Paper in Renewable Energy 9(1-4), September 1996 Conference: Renewable Energy (WREC-96), At London, UK, Volume: II

50. Ramachandra, T. V., Subramanian, D. K., and Joshil N. V. , 1997 “Wind Energy potential and energy potential assessment in Uttara Kannada District of Karnataka, India, Renewable Energy, Vol. 10, No. 4, pp. 585-611, 1997, Elsevier Science Ltd

51. RBZ monetary policy Statement, Sept 2016

52. Reserve Bank Quarterly Review, 2002

53. Riffonneau, Y., S. Bacha, F. Barruel and S. Ploix, “Optimal power flow management for grid connected PV systems with batteries,” IEEE Trans. Sustainable Energy, vol. 2, No. 3, pp. 309-320, July 2011

54. Rosell, J.I., Iba´n˜ ez, M., Modelling power output in photovoltaic modules for outdoor operating conditions. Energy Conversion and Management 47, 2424–2430, 2006.

55. Runyon, Jennifer – Renewable Energy World, Vol 20: Issue 1 Jan/Feb 2017 pp 14

56. Sahira, M. H., and Qureshib, A.H., “Assessment of new and renewable energy resources potential and identification of barriers to their significant utilization in Pakistan”, Elsevier, Renewable and Sustainable Energy Reviews, Volume 12, Issue 1, January 2008, Pages 290-298

57. Shaahid, S. M., and I. El-Amin. 2009. Techno-economic evaluation of off-grid hybrid photovoltaic–diesel–battery power systems for rural electrification in Saudi Arabia—A way forward for sustainable development. Renew. Sustainable Energy Rev. 13: 625–633.

58. Siegel MD, Klein SA, Beckman WA. A simplified method for estimating the monthly average performance of photovoltaic systems. Solar Energy 1981;26:413.

59. STEEL, WILLIAM, Renewable Energy World, Vol 20: Issue 1 Jan/Feb 2017 pp 26

60. Symons, P, “Life Estimation of Lead-Acid Battery Cells for Utility Energy Storage,” Proceedings of the Fifth conference on Batteries for Utility Storage, San Juan, Puerto Rico; July, 1995.

61. U.S. Energy Information Administration (2012). Total Electricity Net Generation International Energy Statistics

62. Wang, C. 2006, “Modeling and control of hybrid wind/photovoltaic/fuel cell distributed generation systems”, Montana State University, Bozeman

63. www.africaprogresspanel.org, accessed 17 April 2017
64. http://www.cliffordpower.com
65. www.CO21.paris.org
66. www.eurobat.org, ASSOCIATION OF EUROPEAN AUTOMOTIVE AND INDUSTRIAL BATTERY MANUFACTURERS accessed 30 May 2017
67. www.sapp.co.zw
68. www.soda-pro.com
69. www.zera.co.zw
70. www.zesa.co.zw
71. www.zetdc.co.zw, Loading Shedding Programme accessed 01 May 2017
72. www.zpc.co.zw, generation statistics as of 09 May 2017

APPENDIX

Appendix 1 – Proposed Time of use for Ruia Mine

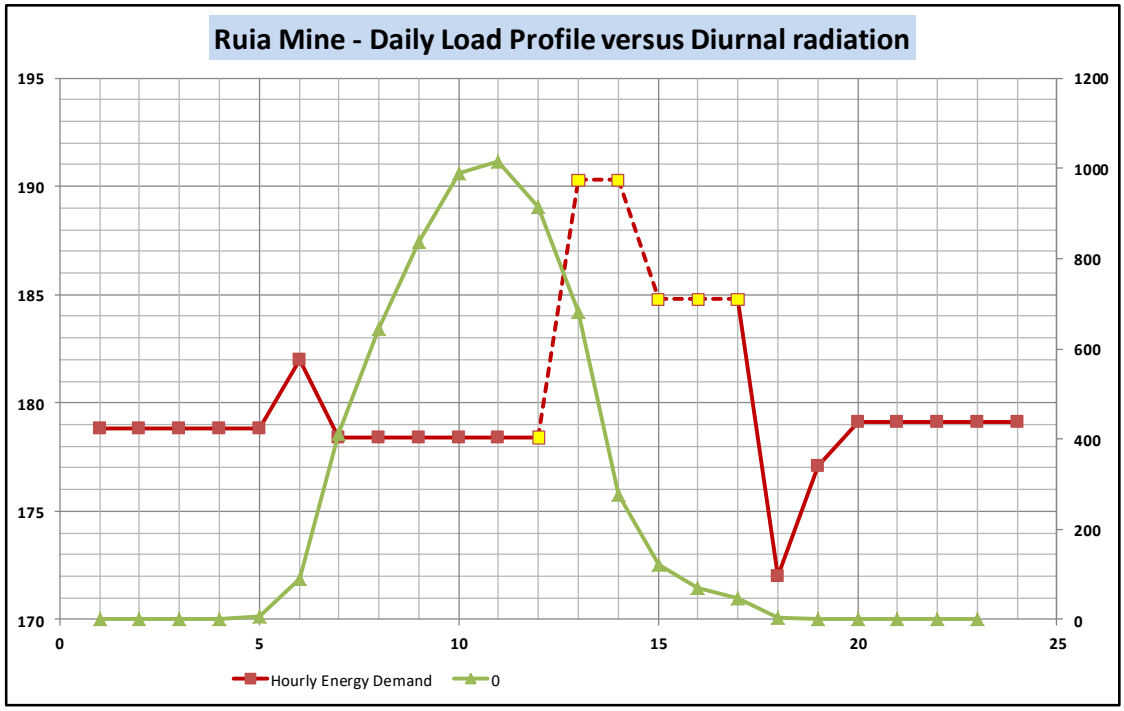

Day of week	0	1	2	3	4	5	6	7	8	9	10	11	12	13	14	15	16	17	18	19	20	21	22	23
Sunday/Holiday																								
Weekday																								
Saturday																								

Appendix 2 – Occurrence of Wet Stacking in Diesel Generators

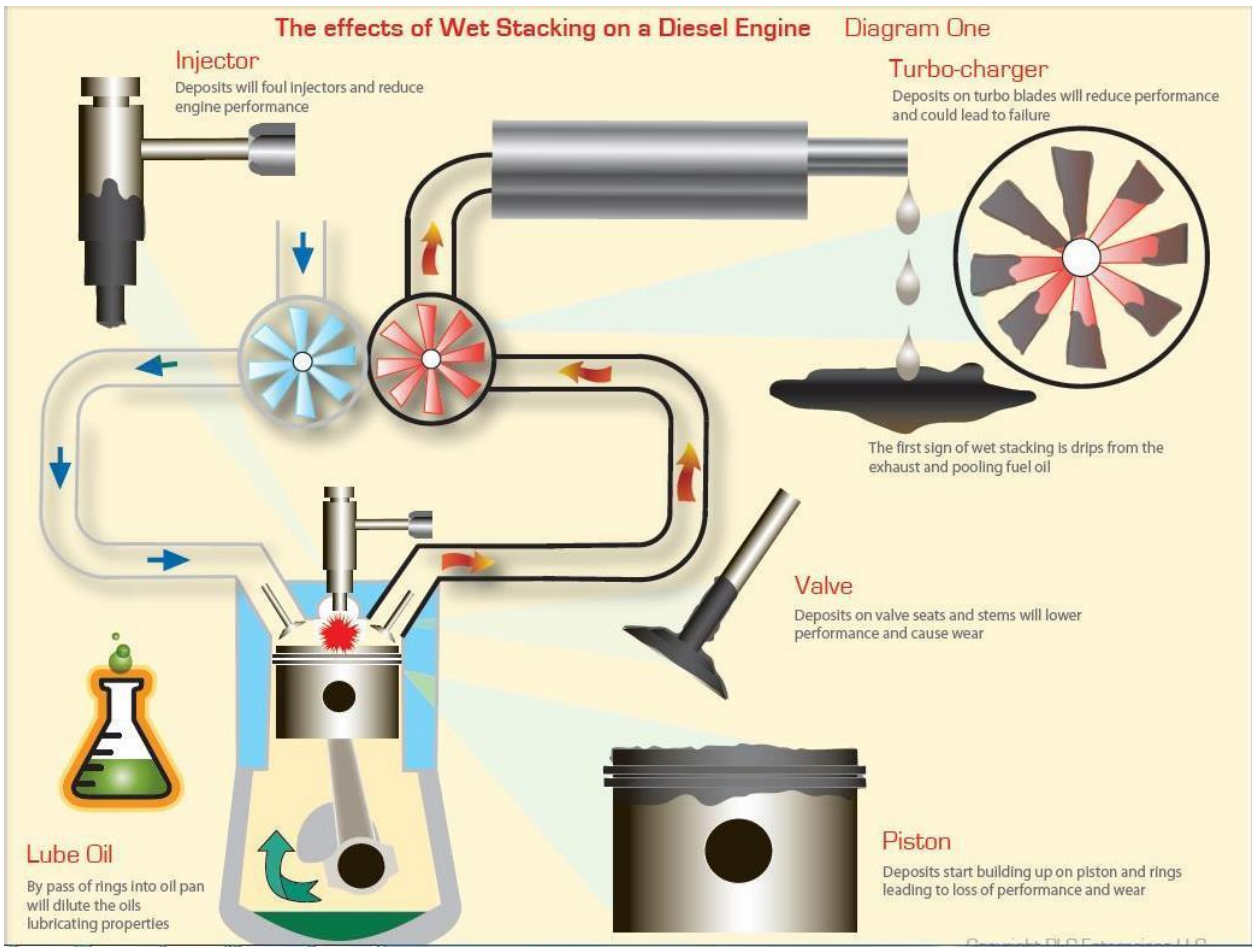

1. http://www.cliffordpower.com/wetstacking.pdf

Appendix 3 – Cummins Diesel generators Technical Specifications

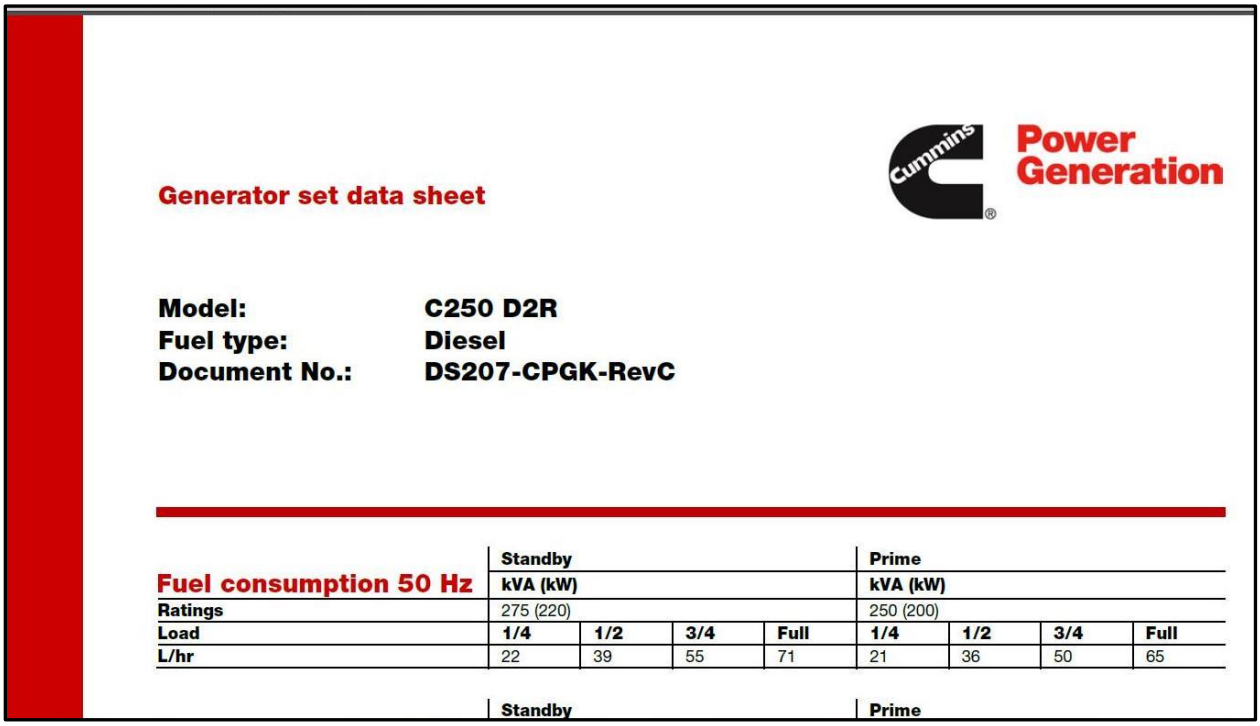

Generator set data sheet

Power Generation

Model: C250 D2R
Fuel type: Diesel
Document No.: DS207-CPGK-RevC

Fuel consumption 50 Hz	Standby				Prime			
	kVA (kW)				kVA (kW)			
Ratings	275 (220)				250 (200)			
Load	1/4	1/2	3/4	Full	1/4	1/2	3/4	Full
L/hr	22	39	55	71	21	36	50	65

	Standby	Prime

2. http://www.raad-eng.com/techdata/cummins/QSK60G3.pdf

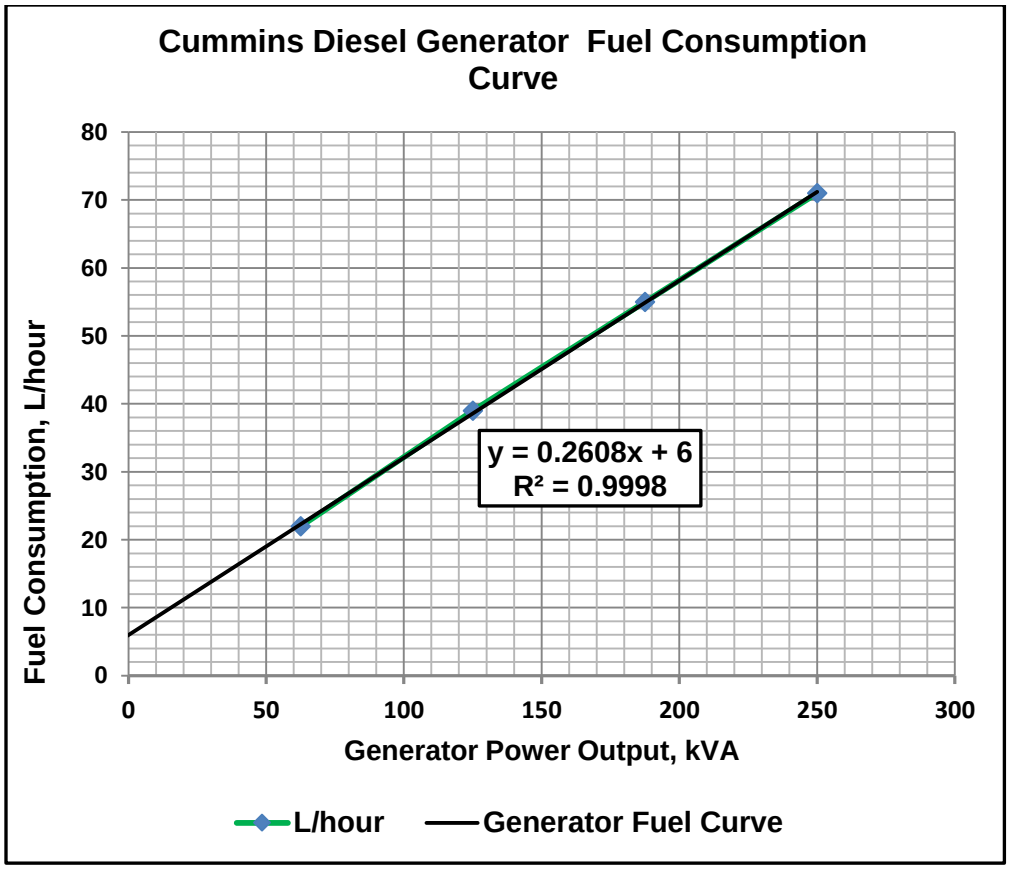
Cummins Diesel Generator Fuel Consumption Curve
Fuel Consumption, L/hour
80
70
60
50
40
30
20
10
0
0
50
100
150
200
250
300
Generator Power Output, kVA
y = 0.2608x + 6
R² = 0.9998
L/hour
Generator Fuel Curve

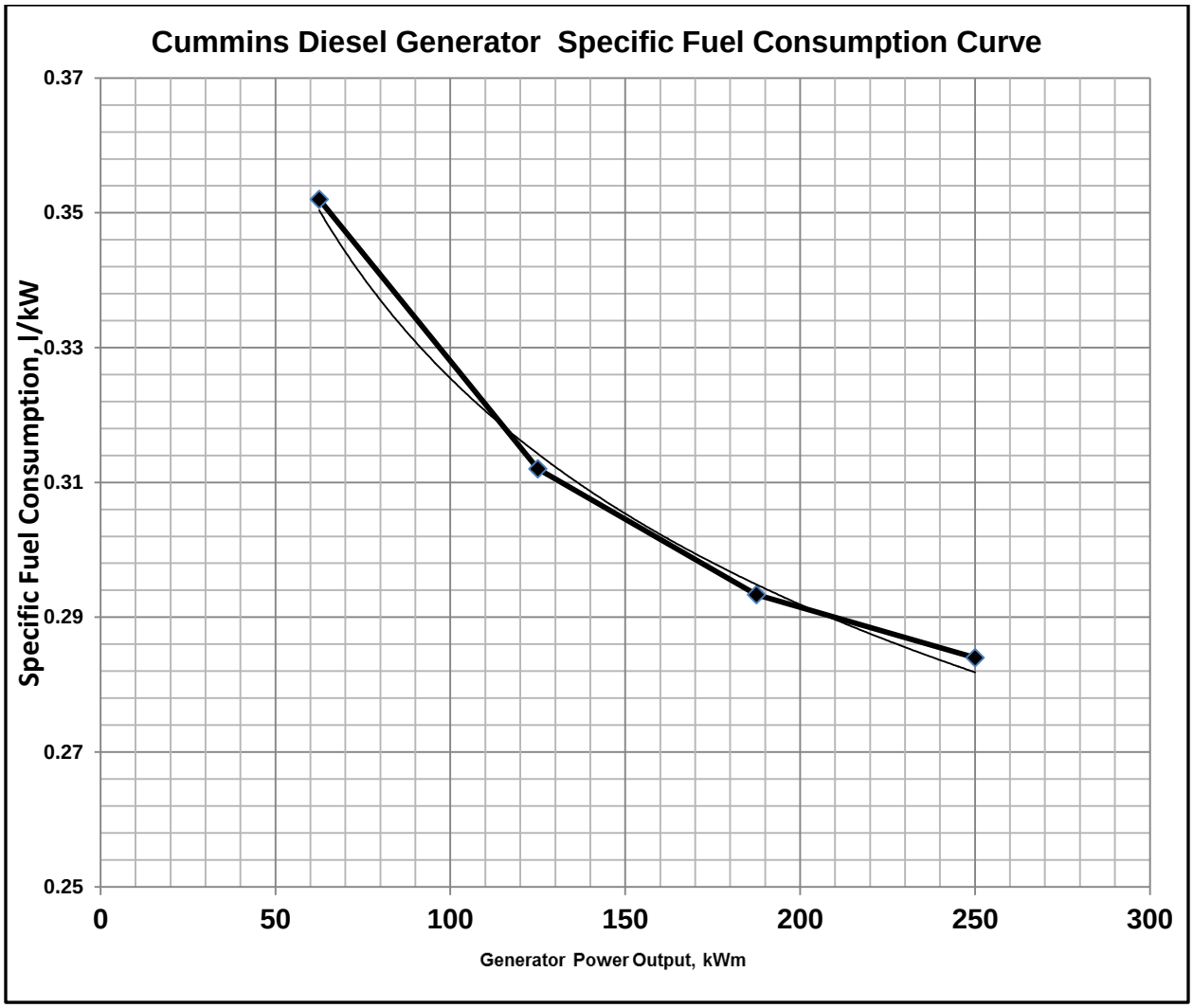
Cummins Diesel Generator Specific Fuel Consumption Curve
Specific Fuel Consumption, l/kW
0.37
0.35
0.33
0.31
0.29
0.27
0.25
0
50
100
150
200
250
300
Generator Power Output, kWm

Appendix 4 – Fuel Price Structure

Fuel Pricing Formulas

SCHEDULE (*Section 6*)

Part I

DIESEL PRICING STRUCTURE

ZERA – DIESEL PRICING STRUCTURE			
		US$	**Price (US$)**
1	FOB Price	a	
2	Freight	b	0.0655
3	Total Landed Cost	(a+b) = C	
4	TAXES & LEVIES		
5	Duty	d	0.40 for diesel
6	Zinara road levy	e	0.06 for diesel
7	Carbon tax	f	0.013 for diesel
8	Debt redemption	g	0.013 for diesel
9	Strategic Reserve Levy	h	0.015
10	Total taxes & levies	(d+e+f+g+h) = I	
11	ADMNISTRATIVE COSTS		
12	Storage and Handling	j	0.015 for diesel
13	Clearing Agency fee	k	0.001 for diesel
14	Financing cost	l	0.010 for diesel
16	Total administrative costs	(j+k+l) = M	
17	Total product cost – Depot	C + I + M	
18	DISTRIBUTION COSTS		
19	Inland bridging cost	p	0.015 for diesel
20	Storage and handling costs	q	0.015 for diesel
21	Secondary transport cost	r	0.020 for diesel
22	Total distribution costs	(p+q+r) = S	
23	Oil Company Purchase Price	C +I +M + S = T	
24	Oil Company margin (7%)	T * 0.07 = U	
25	Oil Company Gross proceeds	T + U = V	
26	Dealer Margin (7%)	V* 0.07 = W	US$ 0.06 minimum
27	Final Pump Price	V + W = X	

Statutory Instrument 80 of 2014, Petroleum (Fuels Pricing) Regulation, 2013 was made in terms of Section 57 of the Petroleum Act [Chapter 13:22] and it gives the following fuel Pricing Structure: **www.zera.co.zw**

Landed Price model of diesel at NOCZIM depot: P/L diesel = a + 0.693

a = FOB price / L

Appendix 4 – Monthly Meteorological Data for Ruia Mine

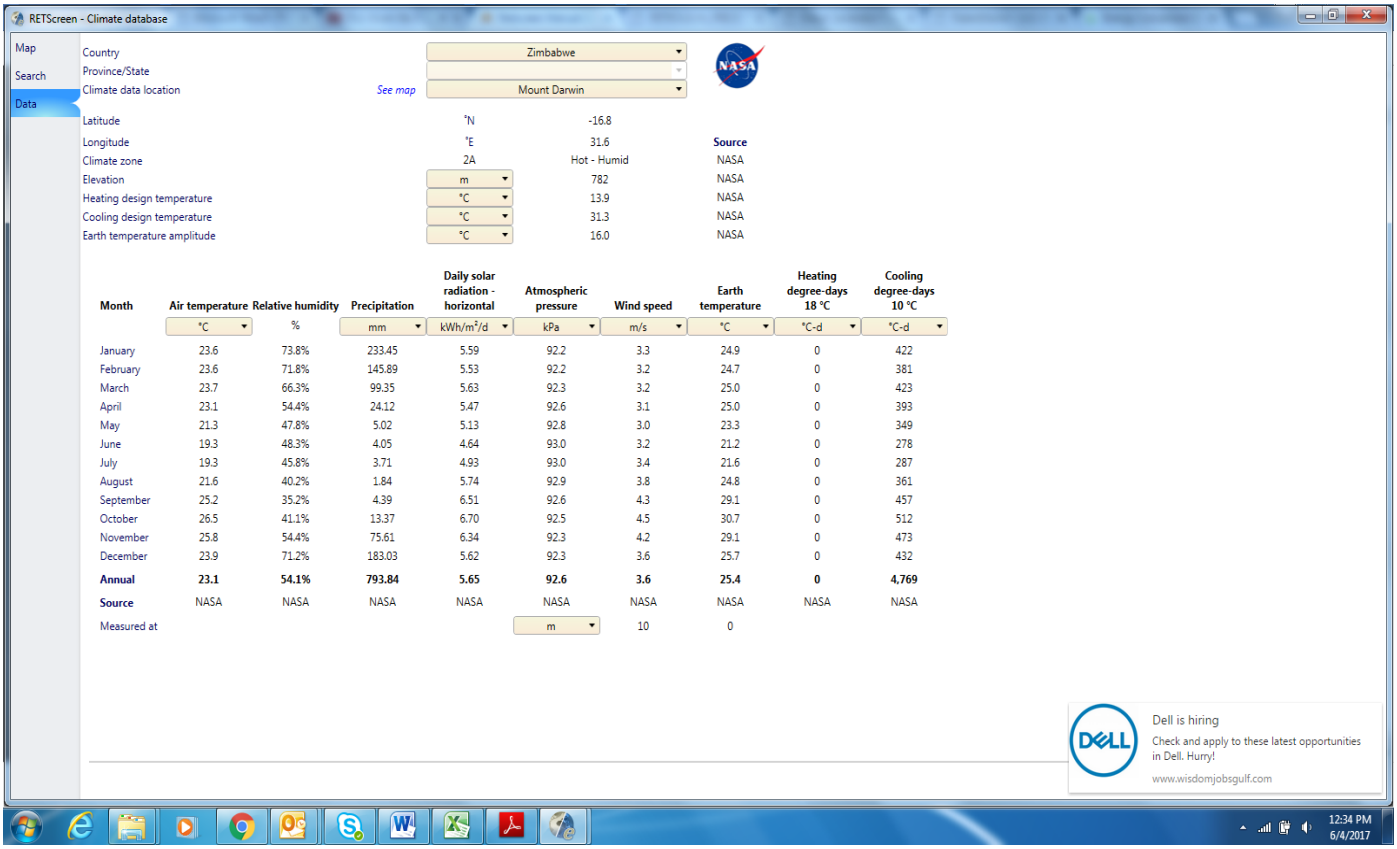

www.retscreen.com